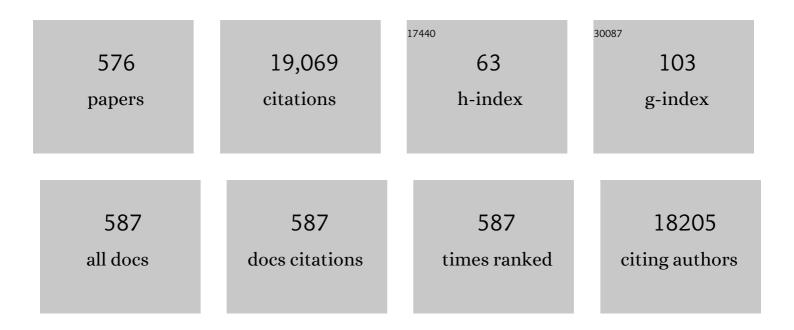
## List of Publications by Year in descending order

Source: https://exaly.com/author-pdf/4436/publications.pdf Version: 2024-02-01



| #  | Article  | IF   | CITATIONS |
|----|--|------|-----------|
| 1  | End-to-End Optimized Versatile Image Compression With Wavelet-Like Transform. IEEE Transactions on<br>Pattern Analysis and Machine Intelligence, 2022, 44, 1247-1263.  | 13.9 | 61        |
| 2  | Nanostructure and reactivity of soot from biofuel 2,5-dimethylfuran pyrolysis with CO2 additions.<br>Frontiers in Energy, 2022, 16, 292-306.   | 2.3  | 10        |
| 3  | E-Commerce Storytelling Recommendation Using Attentional Domain-Transfer Network and Adversarial Pre-Training. IEEE Transactions on Multimedia, 2022, 24, 506-518.   | 7.2  | 6         |
| 4  | Tradeoff Between Robustness and Functionality in Cyber-Coupled Power Systems. IEEE Systems Journal, 2022, 16, 499-509.   | 4.6  | 4         |
| 5  | Spatiotemporal Generative Adversarial Network-Based Dynamic Texture Synthesis for Surveillance<br>Video Coding. IEEE Transactions on Circuits and Systems for Video Technology, 2022, 32, 359-373.                       | 8.3  | 13        |
| 6  | Large-scale production of holey carbon nanosheets implanted with atomically dispersed Fe sites for boosting oxygen reduction electrocatalysis. Nano Research, 2022, 15, 1926-1933.                                       | 10.4 | 17        |
| 7  | Metal-organic framework assembly derived hierarchically ordered porous carbon for oxygen reduction in both alkaline and acidic media. Chemical Engineering Journal, 2022, 430, 132762.                                   | 12.7 | 13        |
| 8  | Nanostructured hexaazatrinaphthalene based polymers for advanced energy conversion and storage.<br>Chemical Engineering Journal, 2022, 427, 130995.  | 12.7 | 16        |
| 9  | Defect Engineering in Photocatalytic Methane Conversion. Small Structures, 2022, 3, 2100147.   | 12.0 | 43        |
| 10 | Site-density engineering of single-atomic iron catalysts for high-performance proton exchange<br>membrane fuel cells. Applied Catalysis B: Environmental, 2022, 302, 120860.   | 20.2 | 42        |
| 11 | Effects of aluminum addition on flash ignition and combustion of boron nanoparticles. Combustion and Flame, 2022, 236, 111762.   | 5.2  | 12        |
| 12 | Operational characteristics and parameter sensitivity analysis of hydropower unit damping under<br>ultra-low frequency oscillations. International Journal of Electrical Power and Energy Systems, 2022,<br>136, 107689. | 5.5  | 14        |
| 13 | Single-atom-based catalysts for photoelectrocatalysis: challenges and opportunities. Journal of<br>Materials Chemistry A, 2022, 10, 5878-5888.   | 10.3 | 17        |
| 14 | Self-templating synthesis of heteroatom-doped large-scalable carbon anodes for high-performance<br>lithium-ion batteries. Inorganic Chemistry Frontiers, 2022, 9, 1058-1069.   | 6.0  | 72        |
| 15 | Reducing the NOx emissions during NH3 oxidation with Nickel modified Fe2O3-a promising cost-effective and environmentally friendly catalyst for NH3 combustion. Combustion and Flame, 2022, 237, 111845.                 | 5.2  | 10        |
| 16 | Influence of water diversion system topologies and operation scenarios on the damping<br>characteristics of hydropower units under ultra-low frequency oscillations. Energy, 2022, 239,<br>122679.                       | 8.8  | 15        |
| 17 | Effects of oxygenated biofuel additives on soot formation: A comprehensive review of laboratory-scale studies. Fuel, 2022, 313, 122635.  | 6.4  | 31        |
| 18 | Chemical effects of carbon dioxide in ethylene, ethanol and DME counter-flow diffusion flames: An experimental reference for the fictitious CO2 flame. Journal of the Energy Institute, 2022, 100, 245-258.              | 5.3  | 9         |

| #  | Article   | IF   | CITATIONS |
|----|---|------|-----------|
| 19 | 3D interconnected g-C3N4 hybridized with 2D Ti3C2 MXene nanosheets for enhancing visible light<br>photocatalytic hydrogen evolution and dye contaminant elimination. Applied Surface Science, 2022,<br>579, 152180. | 6.1  | 47        |
| 20 | Optimal design of hydro-wind-PV multi-energy complementary systems considering smooth power output. Sustainable Energy Technologies and Assessments, 2022, 50, 101832.  | 2.7  | 14        |
| 21 | Lidar Ratio Regional Transfer Method for Extinction Coefficient Accuracy Improvement in Lidar<br>Networks. Remote Sensing, 2022, 14, 626.   | 4.0  | 0         |
| 22 | Recent Advances in Porous Materials for Photocatalytic CO <sub>2</sub> Reduction. Journal of Physical Chemistry Letters, 2022, 13, 1272-1282.   | 4.6  | 30        |
| 23 | Characteristics of snowmelt transport in farmland soil in cold regions: The regulatory mechanism of biochar. Hydrological Processes, 2022, 36, .  | 2.6  | 4         |
| 24 | Strong Metal–Support Interaction Boosts Activity, Selectivity, and Stability in Electrosynthesis of<br>H <sub>2</sub> O <sub>2</sub> . Journal of the American Chemical Society, 2022, 144, 2255-2263.              | 13.7 | 90        |
| 25 | Effects of High Level of Penetration of Renewable Energy Sources on Cascading Failure of Modern<br>Power Systems. IEEE Journal on Emerging and Selected Topics in Circuits and Systems, 2022, 12, 98-106.           | 3.6  | 16        |
| 26 | Evolving framework of studies on global gulf ecosystems with Sustainable Development Goals.<br>Environmental Science and Pollution Research, 2022, 29, 18385-18397.   | 5.3  | 4         |
| 27 | Efficient Dye Contaminant Elimination and Simultaneously Electricity Production via a Bi-Doped TiO2<br>Photocatalytic Fuel Cell. Nanomaterials, 2022, 12, 210.  | 4.1  | 6         |
| 28 | Anemochore Seeds Harbor Distinct Fungal and Bacterial Abundance, Composition, and Functional<br>Profiles. Journal of Fungi (Basel, Switzerland), 2022, 8, 89.   | 3.5  | 6         |
| 29 | Textile-based moisture power generator with dual asymmetric structure and high flexibility for wearable applications. Nano Energy, 2022, 95, 107017.  | 16.0 | 43        |
| 30 | Enhancing ionic conductivity in tablet–bottlebrush block copolymer electrolytes with well-aligned<br>nanostructures <i>via</i> solvent vapor annealing. Journal of Materials Chemistry C, 2022, 10,<br>4247-4256.   | 5.5  | 4         |
| 31 | Peroxymonosulfate activation by Co3O4/SnO2 for efficient degradation of ofloxacin under visible light. Journal of Colloid and Interface Science, 2022, 615, 650-662.  | 9.4  | 43        |
| 32 | Emerging Stacked Photocatalyst Design Enables Spatially Separated Ni(OH) <sub>2</sub> Redox<br>Cocatalysts for Overall CO <sub>2</sub> Reduction and H <sub>2</sub> O Oxidation. Small, 2022, 18,<br>e2104681.      | 10.0 | 23        |
| 33 | Ordered structure constructed from <i>C</i> <sub>2</sub> -symmetric<br>hexa- <i>peri</i> -hexabenzocoronene linked with oligo(dimethylsiloxane). Soft Matter, 2022, 18,<br>3430-3436.                               | 2.7  | 3         |
| 34 | Nonlinear Behavior and Reduced-Order Models of Islanded Microgrid. IEEE Transactions on Power Electronics, 2022, 37, 9212-9225.   | 7.9  | 4         |
| 35 | Water Cloud Detection with Circular Polarization Lidar: A Semianalytic Monte Carlo Simulation Approach. Sensors, 2022, 22, 1679.  | 3.8  | 2         |
| 36 | Research on the Operational Strategy of the Hybrid Wind/PV/Small-Hydropower/Facility-Agriculture<br>System Based on a Microgrid. Energies, 2022, 15, 2466.  | 3.1  | 4         |

| #  | Article   | IF   | CITATIONS |
|----|---|------|-----------|
| 37 | MicroRNA-22 coordinates vascular and motor neuronal pathfinding via <i>sema4</i> during zebrafish development. Open Biology, 2022, 12, 210315.  | 3.6  | 0         |
| 38 | Utilization of carbon-based energy as raw material instead of fuel with low CO2 emissions: Energy<br>analyses and process integration of chemical looping ammonia generation. Applied Energy, 2022, 312,<br>118809. | 10.1 | 11        |
| 39 | Facile synthesis of three-dimensional hollow porous carbon doped polymeric carbon nitride with highly efficient photocatalytic performance. Chemical Engineering Journal, 2022, 438, 135623.                        | 12.7 | 74        |
| 40 | Boosting Li-CO2 battery performances by creating holey structure on CNT cathodes. Electrochimica Acta, 2022, 417, 140310.   | 5.2  | 12        |
| 41 | Hopf Bifurcation and Parameter Sensitivity Analysis of a Doubly-Fed Variable-Speed Pumped Storage<br>Unit. Energies, 2022, 15, 204.   | 3.1  | 4         |
| 42 | Geometrically Deformed Iron-Based Single-Atom Catalysts for High-Performance Acidic Proton<br>Exchange Membrane Fuel Cells. ACS Catalysis, 2022, 12, 5397-5406.   | 11.2 | 43        |
| 43 | Photocatalytic Inactivation of Bacillus subtilis Spores by Natural Sphalerite with Persulfate under<br>Visible Light Irradiation. Coatings, 2022, 12, 528.  | 2.6  | 1         |
| 44 | Attribute Artifacts Removal for Geometry-Based Point Cloud Compression. IEEE Transactions on Image Processing, 2022, 31, 3399-3413.   | 9.8  | 9         |
| 45 | Probing sooting limits in counterflow diffusion flames via multiple optical diagnostic techniques.<br>Experimental Thermal and Fluid Science, 2022, 136, 110679.  | 2.7  | 0         |
| 46 | In-situ construction of chemically bonded conductive polymeric network for high-performance silicon microparticle anodes in lithium-ion batteries. Journal of Power Sources, 2022, 539, 231591.                     | 7.8  | 12        |
| 47 | Effects of Volumetric Property Models on the Efficiency of a Porous Volumetric Solar Receiver.<br>Energies, 2022, 15, 3899.   | 3.1  | 3         |
| 48 | Quantitative optical diagnostics on macroscopic soot onset for ethylene diffusion flames with ethyl ester addition. Optics Express, 2022, 30, 21410.  | 3.4  | 5         |
| 49 | Water-Soluble Conductive Composite Binder for High-Performance Silicon Anode in Lithium-Ion<br>Batteries. Batteries, 2022, 8, 54.   | 4.5  | 8         |
| 50 | Compressed-Encoding Particle Swarm Optimization with Fuzzy Learning for Large-Scale Feature Selection. Symmetry, 2022, 14, 1142.  | 2.2  | 18        |
| 51 | Effects of diluent gases on sooting transition process in ethylene counterflow diffusion flames. RSC<br>Advances, 2022, 12, 18181-18196.  | 3.6  | 2         |
| 52 | Disparity-Aware Reference Frame Generation Network for Multiview Video Coding. IEEE Transactions<br>on Image Processing, 2022, 31, 4515-4526.   | 9.8  | 2         |
| 53 | An integrated modeling framework for cascading failure study and robustness assessment of cyber-coupled power grids. Reliability Engineering and System Safety, 2022, 226, 108654.                                  | 8.9  | 13        |
| 54 | Solar Energy Storage in an All-Vanadium Photoelectrochemical Cell: Structural Effect of Titania<br>Nanocatalyst in Photoanode. Energies, 2022, 15, 4508.  | 3.1  | 2         |

| #  | Article   | lF   | CITATIONS |
|----|---|------|-----------|
| 55 | Effects of flame temperature and radiation properties on infrared light field imaging. Case Studies in<br>Thermal Engineering, 2022, 36, 102215.  | 5.7  | 2         |
| 56 | Expression analysis of nel during zebrafish embryonic development. Gene Expression Patterns, 2022, 45, 119258.  | 0.8  | 1         |
| 57 | Measurements and correlation of hydraulic resistance for H2O/CO2 mixtures at supercritical pressure. International Journal of Heat and Mass Transfer, 2022, 194, 123095.  | 4.8  | 3         |
| 58 | Comprehensive optical diagnostics for flame behavior and soot emission response to a non-equilibrium plasma. Energy, 2022, 255, 124555.   | 8.8  | 4         |
| 59 | Meshed axisymmetric flame simulation and temperature reconstruction using light field camera.<br>Optics and Lasers in Engineering, 2022, 158, 107159.   | 3.8  | 6         |
| 60 | Carbon nanotubes with fluorine-rich surface as metal-free electrocatalyst for effective synthesis of urea from nitrate and CO2. Applied Catalysis B: Environmental, 2022, 316, 121618.  | 20.2 | 62        |
| 61 | A hollow PdCuMoNiCo high-entropy alloy as an efficient bi-functional electrocatalyst for oxygen reduction and formic acid oxidation. Journal of Materials Chemistry A, 2022, 10, 14857-14865.   | 10.3 | 28        |
| 62 | Ultra-stretchable ion gels based on physically cross-linked polymer networks. Journal of Materials<br>Chemistry C, 2022, 10, 10926-10934.   | 5.5  | 4         |
| 63 | Deep High-Resolution Representation Learning for Visual Recognition. IEEE Transactions on Pattern<br>Analysis and Machine Intelligence, 2021, 43, 3349-3364.  | 13.9 | 1,553     |
| 64 | Learning and Fusing Multiple User Interest Representations for Micro-Video and Movie<br>Recommendations. IEEE Transactions on Multimedia, 2021, 23, 484-496.  | 7.2  | 32        |
| 65 | Ensemble Learning-Based Rate-Distortion Optimization for End-to-End Image Compression. IEEE Transactions on Circuits and Systems for Video Technology, 2021, 31, 1193-1207.   | 8.3  | 27        |
| 66 | Deep Adversarial Data Augmentation for Extremely Low Data Regimes. IEEE Transactions on Circuits and Systems for Video Technology, 2021, 31, 15-28.   | 8.3  | 40        |
| 67 | Soot properties in ethylene inverse diffusion flames blended with different carbon chain length<br>alcohols. Fuel, 2021, 287, 119520.   | 6.4  | 18        |
| 68 | Flow field characteristics, mixing and emissions performance of a lab-scale rich-quench-lean<br>trapped-vortex combustor utilizing a quench orifice plate combined with a bluff-body. Chinese<br>Journal of Aeronautics, 2021, 34, 476-492. | 5.3  | 10        |
| 69 | Systematic profiling of early regulators during tissue regeneration using zebrafish model. Wound<br>Repair and Regeneration, 2021, 29, 189-195.   | 3.0  | 5         |
| 70 | Formation and characteristics of soot from pyrolysis of ethylene blended with furan fuels. Science<br>China Technological Sciences, 2021, 64, 585-598.  | 4.0  | 9         |
| 71 | High-performance metal–iodine batteries enabled by a bifunctional dendrite-free Li–Na alloy anode.<br>Journal of Materials Chemistry A, 2021, 9, 538-545.   | 10.3 | 18        |
| 72 | A high-pressure artificial photosynthetic device: pumping carbon dioxide as well as achieving selectivity. Journal of Materials Chemistry A, 2021, 9, 3961-3967.  | 10.3 | 16        |

| #  | Article  | IF   | CITATIONS |
|----|--|------|-----------|
| 73 | Single copper sites dispersed on hierarchically porous carbon for improving oxygen reduction reaction towards zinc-air battery. Nano Research, 2021, 14, 998-1003.   | 10.4 | 50        |
| 74 | Deep Multi-Domain Prediction for 3D Video Coding. IEEE Transactions on Broadcasting, 2021, 67, 813-823.  | 3.2  | 10        |
| 75 | Electrocatalytic generation and tuning of ultra-stable and ultra-dense nanometre bubbles: an <i>in situ</i> molecular dynamics study. Nanoscale, 2021, 13, 11242-11249.  | 5.6  | 6         |
| 76 | A Tutorial on Modeling and Analysis of Cascading Failure in Future Power Grids. IEEE Transactions on Circuits and Systems II: Express Briefs, 2021, 68, 49-55.   | 3.0  | 25        |
| 77 | ls Heuristic Sampling Necessary in Training Deep Object Detectors?. IEEE Transactions on Image<br>Processing, 2021, 30, 8454-8467.   | 9.8  | 6         |
| 78 | Deep Network-Based Frame Extrapolation With Reference Frame Alignment. IEEE Transactions on Circuits and Systems for Video Technology, 2021, 31, 1178-1192.  | 8.3  | 20        |
| 79 | Enhanced visible light photoelectrocatalytic degradation of tetracycline hydrochloride by I and P<br>co-doped TiO2 photoelectrode. Journal of Hazardous Materials, 2021, 406, 124309.  | 12.4 | 70        |
| 80 | Fundamental Insights into Surface Modification of Silicon Material toward Improved Activity and<br>Durability in Photocatalytic Hydrogen Production: A Case Study of Pre-Lithiation. Journal of Physical<br>Chemistry C, 2021, 125, 5542-5548. | 3.1  | 7         |
| 81 | How soil texture, channel shape and crossâ€sectional area affect moisture dynamics and water loss in<br>irrigation channels. Hydrological Processes, 2021, 35, e14155.   | 2.6  | 3         |
| 82 | Plasmonic Coupling Architectures for Enhanced Photocatalysis. Advanced Materials, 2021, 33, e2005738.  | 21.0 | 51        |
| 83 | E2I: Generative Inpainting From Edge to Image. IEEE Transactions on Circuits and Systems for Video Technology, 2021, 31, 1308-1322.  | 8.3  | 48        |
| 84 | An efficient combination strategy for high-performance asymmetric-electrolyte metal–air batteries.<br>Matter, 2021, 4, 1090-1092.  | 10.0 | 5         |
| 85 | Nanopore Sequencing and Hi-C Based De Novo Assembly of Trachidermus fasciatus Genome. Genes, 2021, 12, 692.  | 2.4  | 2         |
| 86 | Nuclear exosome HMGB3 secreted by nasopharyngeal carcinoma cells promotes tumour metastasis by inducing angiogenesis. Cell Death and Disease, 2021, 12, 554.   | 6.3  | 27        |
| 87 | Semantics-to-Signal Scalable Image Compression with Learned Revertible Representations.<br>International Journal of Computer Vision, 2021, 129, 2605-2621.   | 15.6 | 21        |
| 88 | Topological Defectâ€Rich Carbon as a Metalâ€Free Cathode Catalyst for Highâ€Performance<br>Liâ€CO <sub>2</sub> Batteries. Advanced Energy Materials, 2021, 11, 2101390.  | 19.5 | 60        |
| 89 | Damping characteristics analysis of hydropower units under full operating conditions and control parameters: Accurate quantitative evaluation based on refined models. Applied Energy, 2021, 292, 116881.                                      | 10.1 | 24        |
| 90 | SIZ1 regulates phosphate deficiency-induced inhibition of primary root growth of Arabidopsis by<br>modulating Fe accumulation and ROS production in its roots. Plant Signaling and Behavior, 2021, 16,<br>1946921.                             | 2.4  | 3         |

| #   | Article  | IF   | CITATIONS |
|-----|--|------|-----------|
| 91  | 3D interconnected porous g-C3N4 hybridized with Fe2O3 quantum dots for enhanced photo-Fenton performance. Applied Surface Science, 2021, 555, 149677.  | 6.1  | 52        |
| 92  | N, P, and S tri-doped holey carbon as an efficient electrocatalyst for oxygen reduction in whole pH range for fuel cell and zinc-air batteries. Carbon, 2021, 179, 365-376.  | 10.3 | 47        |
| 93  | Self-Healing Solid Polymer Electrolyte with High Ion Conductivity and Super Stretchability for All-Solid Zinc-Ion Batteries. ACS Applied Materials & Interfaces, 2021, 13, 36320-36329.                                | 8.0  | 42        |
| 94  | Nonlinear modeling and multi-scale damping characteristics of hydro-turbine regulation systems<br>under complex variable hydraulic and electrical network structures. Applied Energy, 2021, 293, 116949.               | 10.1 | 28        |
| 95  | The Curing Kinetics Analysis of Four Epoxy Resins Using a Diamine Terminated Polyether as Curing<br>Agent. Thermochimica Acta, 2021, 702, 178987.  | 2.7  | 14        |
| 96  | Revisiting seasonal dynamics of total nitrogen in reservoirs with a systematic framework for mining data from existing publications. Water Research, 2021, 201, 117380.  | 11.3 | 7         |
| 97  | On the treatment of lens optical center uncertainty in simultaneous reconstruction of flame temperature and soot volume fraction distributions by a CCD camera. Optik, 2021, 241, 167238.                              | 2.9  | 3         |
| 98  | Simultaneously Engineering the Coordination Environment and Pore Architecture of Metal–Organic<br>Frameworkâ€Derived Singleâ€Atomic Iron Catalysts for Ultraefficient Oxygen Reduction. Small, 2021, 17,<br>e2102425.  | 10.0 | 49        |
| 99  | Experimental and numerical study on sooting transition process in iso-octane counterflow diffusion flames: Diagnostics and combustion chemistry. Journal of the Energy Institute, 2021, 98, 282-293.                   | 5.3  | 10        |
| 100 | Boron, nitrogen co-doped carbon with abundant mesopores for efficient CO2 electroreduction.<br>Applied Catalysis B: Environmental, 2021, 298, 120543.  | 20.2 | 61        |
| 101 | New species of the subgenus <i>Hoplophorella</i> (Oribatida: Steganacaridae: <i>Atropacarus</i> )<br>from South China. International Journal of Acarology, 2021, 47, 89-94.  | 0.7  | 0         |
| 102 | Deep Learning-Based Video Coding. ACM Computing Surveys, 2021, 53, 1-35.   | 23.0 | 78        |
| 103 | SSSIC: Semantics-to-Signal Scalable Image Coding With Learned Structural Representations. IEEE Transactions on Image Processing, 2021, 30, 8939-8954.  | 9.8  | 13        |
| 104 | Context-Adaptive Inverse Quantization for Inter-Frame Coding. IEEE Open Journal of Circuits and Systems, 2021, 2, 660-674.   | 1.9  | 1         |
| 105 | Sub-5 nm homeotropically aligned columnar structures of hybrids constructed by porphyrin and oligo(dimethylsiloxane). Chemical Communications, 2021, 58, 108-111.  | 4.1  | 3         |
| 106 | Soil Rehabilitation Promotes Resilient Microbiome with Enriched Keystone Taxa than Agricultural<br>Infestation in Barren Soils on the Loess Plateau. Biology, 2021, 10, 1261.  | 2.8  | 4         |
| 107 | Nonstationary Shape Estimation in Electrical Impedance Tomography Using a Parametric Level<br>Set-Based Extended Kalman Filter Approach. IEEE Transactions on Instrumentation and Measurement,<br>2020, 69, 1894-1907. | 4.7  | 40        |
| 108 | Light Field Super-Resolution By Jointly Exploiting Internal and External Similarities. IEEE Transactions<br>on Circuits and Systems for Video Technology, 2020, 30, 2604-2616.   | 8.3  | 29        |

| #   | Article  | IF   | CITATIONS |
|-----|--|------|-----------|
| 109 | Combustion of single particles from sewage sludge/pine sawdust and sewage sludge/bituminous coal under oxy-fuel conditions with steam addition. Waste Management, 2020, 101, 1-8.  | 7.4  | 30        |
| 110 | Interferometric measurement of freeform surfaces using irregular subaperture stitching.<br>Measurement Science and Technology, 2020, 31, 055202.   | 2.6  | 6         |
| 111 | Comparative study on characteristics of soot from n-decane and RP-3 kerosene normal/inverse diffusion flames. Journal of the Energy Institute, 2020, 93, 62-75.  | 5.3  | 21        |
| 112 | Quadtree-Based Coding Framework for High-Density Camera Array-Based Light Field Image. IEEE<br>Transactions on Circuits and Systems for Video Technology, 2020, 30, 2694-2708.   | 8.3  | 5         |
| 113 | The study of co-combustion characteristics of coal and microalgae by single particle combustion and TGA methods. Journal of the Energy Institute, 2020, 93, 508-517.   | 5.3  | 34        |
| 114 | Deep Learning-Based Technology in Responses to the Joint Call for Proposals on Video Compression<br>With Capability Beyond HEVC. IEEE Transactions on Circuits and Systems for Video Technology, 2020,<br>30, 1267-1280. | 8.3  | 31        |
| 115 | Deep Learning-Based Classification of Liver Cancer Histopathology Images Using Only Global Labels.<br>IEEE Journal of Biomedical and Health Informatics, 2020, 24, 1643-1651.  | 6.3  | 71        |
| 116 | Frank-Wolfe Network: An Interpretable Deep Structure for Non-Sparse Coding. IEEE Transactions on Circuits and Systems for Video Technology, 2020, 30, 3068-3080.   | 8.3  | 8         |
| 117 | iWave: CNN-Based Wavelet-Like Transform for Image Compression. IEEE Transactions on Multimedia, 2020, 22, 1667-1679.   | 7.2  | 42        |
| 118 | Promising zirconia-mixed Al-based nitrogen carriers for chemical looping of NH3: Reduced NH3 decomposition and improved NH3 yield. Fuel, 2020, 264, 116821.  | 6.4  | 24        |
| 119 | Soot formation and combustion characteristics in confined mesoscale combustors under conventional and oxy-combustion conditions (O2/N2 and O2/CO2). Fuel, 2020, 264, 116808.   | 6.4  | 13        |
| 120 | Character-Oriented Video Summarization With Visual and Textual Cues. IEEE Transactions on Multimedia, 2020, 22, 2684-2697.   | 7.2  | 11        |
| 121 | Detection of Chlorophyll a and CDOM Absorption Coefficient with a Dual-Wavelength Oceanic Lidar:<br>Wavelength Optimization Method. Remote Sensing, 2020, 12, 3021.  | 4.0  | 5         |
| 122 | States, Trends, and Future of Aquaponics Research. Sustainability, 2020, 12, 7783.   | 3.2  | 10        |
| 123 | Surface Reconstruction and Phase Transition on Vanadium–Cobalt–Iron Trimetal Nitrides to Form<br>Active Oxyhydroxide for Enhanced Electrocatalytic Water Oxidation. Advanced Energy Materials,<br>2020, 10, 2002464.     | 19.5 | 155       |
| 124 | Highly improved electrocatalytic activity of NiSx: Effects of Cr-doping and phase transition. Applied<br>Catalysis B: Environmental, 2020, 267, 118721.  | 20.2 | 68        |
| 125 | Nanoscale inspection on carbon particles from commercial RP-3 kerosene combustion with different dilutions. Fullerenes Nanotubes and Carbon Nanostructures, 2020, 28, 959-972.   | 2.1  | 4         |
| 126 | Comparative study on soot characteristics of non-swirling and swirling inverse diffusion iso-octane<br>flames with biofuel 2,5-dimethylfuran addition. Journal of the Energy Institute, 2020, 93, 2108-2123.             | 5.3  | 3         |

| #   | Article  | IF   | CITATIONS |
|-----|--|------|-----------|
| 127 | Using Coal Coke for N-Sorption with an Al-based Nitrogen Carrier during Chemical Looping Ammonia<br>Generation. Energy & Fuels, 2020, 34, 12527-12534.   | 5.1  | 7         |
| 128 | A Comprehensive Benchmark for Single Image Compression Artifact Reduction. IEEE Transactions on<br>Image Processing, 2020, 29, 7845-7860.  | 9.8  | 34        |
| 129 | Circuits and Systems Issues in Power Electronics Penetrated Power Grid. IEEE Open Journal of Circuits and Systems, 2020, 1, 140-156.   | 1.9  | 43        |
| 130 | Performance Evaluation of Spaceborne Integrated Path Differential Absorption Lidar for Carbon Dioxide Detection at 1572 nm. Remote Sensing, 2020, 12, 2570.  | 4.0  | 6         |
| 131 | Fault Diagnosis of Rotating Machinery Based on Convolutional Neural Network and Singular Value Decomposition. Shock and Vibration, 2020, 2020, 1-13.   | 0.6  | 5         |
| 132 | A Semianalytic Monte Carlo Simulator for Spaceborne Oceanic Lidar: Framework and Preliminary<br>Results. Remote Sensing, 2020, 12, 2820.   | 4.0  | 11        |
| 133 | Nitrogen, Sulfur Co-Doped Hierarchically Porous Carbon as a Metal-Free Electrocatalyst for Oxygen<br>Reduction and Carbon Dioxide Reduction Reaction. ACS Applied Materials & Interfaces, 2020, 12,<br>44578-44587.                | 8.0  | 69        |
| 134 | Comparative Study on Soot Reduction, Soot Nanostructure and Oxidation Reactivity of<br>n-heptane/DMC and Isooctane/DMC Inverse Diffusion Flames. Journal of Thermal Science, 2020, 29,<br>1269-1281.                               | 1.9  | 3         |
| 135 | Multiple Features Fusion Attention Mechanism Enhanced Deep Knowledge Tracing for Student<br>Performance Prediction. IEEE Access, 2020, 8, 194894-194903.   | 4.2  | 22        |
| 136 | Partition-Aware Adaptive Switching Neural Networks for Post-Processing in HEVC. IEEE Transactions on Multimedia, 2020, 22, 2749-2763.  | 7.2  | 38        |
| 137 | PLD-fabricated perovskite oxide nanofilm as efficient electrocatalyst with highly enhanced water oxidation performance. Applied Catalysis B: Environmental, 2020, 272, 119046.   | 20.2 | 29        |
| 138 | <strong>Contribution to the knowledge of the ptyctimous mite genus<br/><em>Austrophthiracarus</em> (Acari, Oribatida, Steganacaridae) with descriptions of two new<br/>species from China</strong> . Zootaxa, 2020, 4786, 138-144. | 0.5  | 0         |
| 139 | Block Copolymer Electrolytes with Excellent Properties in a Wide Temperature Range. ACS Applied Energy Materials, 2020, 3, 6536-6543.  | 5.1  | 16        |
| 140 | A facile approach to high-performance trifunctional electrocatalysts by substrate-enhanced electroless deposition of Pt/NiO/Ni on carbon nanotubes. Nanoscale, 2020, 12, 14615-14625.  | 5.6  | 32        |
| 141 | Soot particles diagnostics in ethylene inverse diffusion flame blending with biodiesel surrogates of saturated methyl butyrate and unsaturated methyl crotonate. Fuel Processing Technology, 2020, 202, 106379.                    | 7.2  | 16        |
| 142 | A compact Cas9 ortholog from Staphylococcus Auricularis (SauriCas9) expands the DNA targeting scope. PLoS Biology, 2020, 18, e3000686.   | 5.6  | 96        |
| 143 | Construction of Nighttime Cloud Layer Height and Classification of Cloud Types. Remote Sensing, 2020, 12, 668.   | 4.0  | 7         |
| 144 | Graph-Based Non-Convex Low-Rank Regularization for Image Compression Artifact Reduction. IEEE<br>Transactions on Image Processing, 2020, 29, 5374-5385.  | 9.8  | 15        |

| #   | Article   | IF   | CITATIONS |
|-----|---|------|-----------|
| 145 | Compressed Image Restoration via Artifacts-Free PCA Basis Learning and Adaptive Sparse Modeling. IEEE<br>Transactions on Image Processing, 2020, 29, 7399-7413.   | 9.8  | 12        |
| 146 | Ultrathin-metal-film-based transparent electrodes with relative transmittance surpassing 100%.<br>Nature Communications, 2020, 11, 3367.  | 12.8 | 123       |
| 147 | High-performance mesoporous (AlN/Al2O3) for enhanced NH3 yield during chemical looping ammonia generation technology. International Journal of Hydrogen Energy, 2020, 45, 9903-9913.  | 7.1  | 23        |
| 148 | Robust Deep Co-Saliency Detection With Group Semantic and Pyramid Attention. IEEE Transactions on Neural Networks and Learning Systems, 2020, 31, 1-11.   | 11.3 | 25        |
| 149 | Global pattern of studies on phosphorus at watershed scale. Environmental Science and Pollution Research, 2020, 27, 14872-14882.  | 5.3  | 5         |
| 150 | Nitrogen-rich holey graphene for efficient oxygen reduction reaction. Carbon, 2020, 162, 66-73.   | 10.3 | 71        |
| 151 | Formation and nanoscale-characteristics of soot from pyrolysis of ethylene blended with ethanol/dimethyl ether. Journal of the Energy Institute, 2020, 93, 1288-1304.   | 5.3  | 7         |
| 152 | Zero-Shot Depth Estimation From Light Field Using A Convolutional Neural Network. IEEE<br>Transactions on Computational Imaging, 2020, 6, 682-696.  | 4.4  | 40        |
| 153 | Soot formation and evolution in RP-3 kerosene inverse diffusion flames: Effects of flow rates and dimethyl carbonate additions. Fuel, 2020, 273, 117732.  | 6.4  | 15        |
| 154 | Thermodynamic and economic analyses of a coal and biomass indirect coupling power generation system. Frontiers in Energy, 2020, 14, 590-606.  | 2.3  | 5         |
| 155 | Automatic estimation of dairy cattle body condition score from depth image using ensemble model.<br>Biosystems Engineering, 2020, 194, 16-27.   | 4.3  | 27        |
| 156 | A molding method of Na2CO3/Al2O3 sorbents with high sphericity and low roughness for enhanced attrition resistance in CO2 sorption/desorption process via extrusion-spheronization method. Powder Technology, 2020, 366, 520-526. | 4.2  | 9         |
| 157 | Effects of Magnetic Fields on Morphology and Nanostructure Evolution of Incipient Soot Particles from n-heptane/2,5-dimethylfuran Inverse Diffusion Flames. Journal of Thermal Science, 2020, 29, 820-839.                        | 1.9  | 4         |
| 158 | Stability analysis of hydropower units under full operating conditions considering turbine nonlinearity. Renewable Energy, 2020, 154, 723-742.  | 8.9  | 32        |
| 159 | A computer vision-based method for spatial-temporal action recognition of tail-biting behaviour in group-housed pigs. Biosystems Engineering, 2020, 195, 27-41.   | 4.3  | 70        |
| 160 | Morphology and Nanostructure Transitions of Soot with Various Dimethyl Ether Additions in<br>Nonpremixed Ethylene Flames at Different Scales. Energy & Fuels, 2020, 34, 16705-16719.  | 5.1  | 14        |
| 161 | Instrument response effects on the retrieval of oceanic lidar. Applied Optics, 2020, 59, C21.   | 1.8  | 7         |
| 162 | The <i>slc4a2b</i> gene is required for hair cell development in zebrafish. Aging, 2020, 12,<br>18804-18821.  | 3.1  | 41        |

| #   | Article   | IF   | CITATIONS |
|-----|---|------|-----------|
| 163 | <p class="Body"><strong>New findings of ptyctimous mites of the family Steganacaridae<br/>(Acari, Oribatida, Phthiracaroidea) from Yunnan Province, Southwest China</strong></p> .<br>Systematic and Applied Acarology, 2020, 25, 658-667.                          | 0.5  | 1         |
| 164 | Neuronal Population Reconstruction From Ultra-Scale Optical Microscopy Images via Progressive Learning. IEEE Transactions on Medical Imaging, 2020, 39, 4034-4046.  | 8.9  | 14        |
| 165 | The Network Representation Learning Algorithm Based on Semi-Supervised Random Walk. IEEE Access, 2020, 8, 222956-222965.  | 4.2  | 4         |
| 166 | Arphthicarus olszanowskii sp. nov. (Acari: Oribatida: Steganacaridae) from Tibet, China with a Key to<br>Known Species of Arphthicarus from the Palaearctic and Oriental Regions. Annales Zoologici, 2020,<br>70, .   | 0.8  | 0         |
| 167 | Semisupervised Community Preserving Network Embedding with Pairwise Constraints. Complexity, 2020, 2020, 1-14.  | 1.6  | 1         |
| 168 | Detailed investigation of the iterative analysis for inertial confinement fusion target characterization. Applied Optics, 2020, 59, 10880.  | 1.8  | 1         |
| 169 | A Parametric Level Set-Based Approach to Difference Imaging in Electrical Impedance Tomography. IEEE<br>Transactions on Medical Imaging, 2019, 38, 145-155.   | 8.9  | 57        |
| 170 | EFFECTS OF NITRITE ANIONS ON SURFACE PASSIVE FILM PROPERTIES FOR Q235 CARBON STEELS. Surface Review and Letters, 2019, 26, 1850218.   | 1.1  | 14        |
| 171 | Lidar Remote Sensing of Seawater Optical Properties: Experiment and Monte Carlo Simulation. IEEE Transactions on Geoscience and Remote Sensing, 2019, 57, 9489-9498.  | 6.3  | 33        |
| 172 | Transparent Perfect Microwave Absorber Employing Asymmetric Resonance Cavity. Advanced Science, 2019, 6, 1901320.   | 11.2 | 40        |
| 173 | Side-chain effects on the properties of highly branched imidazolium-functionalized copolymer anion exchange membranes. Applied Surface Science, 2019, 493, 1306-1316.   | 6.1  | 29        |
| 174 | Nanowire Photoelectrochemistry. Chemical Reviews, 2019, 119, 9221-9259.   | 47.7 | 158       |
| 175 | Cascading Failure of Cyber-Coupled Power Systems Considering Interactions Between Attack and Defense. IEEE Transactions on Circuits and Systems I: Regular Papers, 2019, 66, 4323-4336.   | 5.4  | 32        |
| 176 | Validation of the Analytical Model of Oceanic Lidar Returns: Comparisons with Monte Carlo<br>Simulations and Experimental Results. Remote Sensing, 2019, 11, 1870.  | 4.0  | 19        |
| 177 | Detection of aggressive behaviours in pigs using a RealSence depth sensor. Computers and Electronics in Agriculture, 2019, 166, 105003.   | 7.7  | 48        |
| 178 | <p class="Body"><strong>Contribution to the knowledge of the oribatid mite genus<br/><em>Apoplophora</em> (Acari, Oribatida, Apoplophoridae) with description of a new species<br/>from China</strong></p> . Systematic and Applied Acarology, 2019, 24, 1911-1917. | 0.5  | 0         |
| 179 | Micro- and nano-structure evolution of soot from isooctane and 2,5-dimethylfuran flames in photocatalytic degradation. Fullerenes Nanotubes and Carbon Nanostructures, 2019, 27, 978-993.   | 2.1  | 4         |
| 180 | Facile Synthesis of FeS@C Particles Toward High-Performance Anodes for Lithium-Ion Batteries.<br>Nanomaterials, 2019, 9, 1467.  | 4.1  | 5         |

| #   | Article   | IF   | CITATIONS |
|-----|---|------|-----------|
| 181 | Cobalt/titanium nitride@N-doped carbon hybrids for enhanced electrocatalytic hydrogen evolution and supercapacitance. New Journal of Chemistry, 2019, 43, 14518-14526.  | 2.8  | 17        |
| 182 | Hoplophthiracarus sidorchukae sp. nov. (Acari, Oribatida, Phthiracaridae) from the North Island, New<br>Zealand. Zootaxa, 2019, 4647, 226-230.  | 0.5  | 2         |
| 183 | A semianalytic Monte Carlo radiative transfer model for polarized oceanic lidar: Experiment-based comparisons and multiple scattering effects analyses. Journal of Quantitative Spectroscopy and Radiative Transfer, 2019, 237, 106638. | 2.3  | 21        |
| 184 | Nanostructure and reactivity of nascent carbon particles from 2,5-dimethylfuran/n-heptane swirling inverse diffusion flames. Fullerenes Nanotubes and Carbon Nanostructures, 2019, 27, 106-119.   | 2.1  | 6         |
| 185 | Synthesis of carbon nanotubes on metal mesh in inverse diffusion biofuel flames. Fullerenes<br>Nanotubes and Carbon Nanostructures, 2019, 27, 77-86.  | 2.1  | 6         |
| 186 | Inverse radiation problem of multi-nanoparticles temperature and concentration fields reconstruction in nanofluid fuel flame. Optik, 2019, 181, 81-91.  | 2.9  | 4         |
| 187 | Spherical Coordinates Transform-Based Motion Model for Panoramic Video Coding. IEEE Journal on Emerging and Selected Topics in Circuits and Systems, 2019, 9, 98-109.   | 3.6  | 15        |
| 188 | A Moving Morphable Components Based Shape Reconstruction Framework for Electrical Impedance<br>Tomography. IEEE Transactions on Medical Imaging, 2019, 38, 2937-2948.   | 8.9  | 44        |
| 189 | Influences of NH 4 + ions and thin electrolyte layers (TEL) thickness on the corrosion behavior of<br>AZ91D magnesium alloy. Materials and Corrosion - Werkstoffe Und Korrosion, 2019, 70, 2088-2102.                                   | 1.5  | 1         |
| 190 | Highly branched poly(arylene ether)/surface functionalized fullereneâ€based composite membrane<br>electrolyte for DMFC applications. International Journal of Energy Research, 2019, 43, 3756-3767.                                     | 4.5  | 24        |
| 191 | Robustness Assessment and Enhancement of Power Grids From a Complex Network's Perspective Using Decision Trees. IEEE Transactions on Circuits and Systems II: Express Briefs, 2019, 66, 833-837.  | 3.0  | 8         |
| 192 | Invertibility-Driven Interpolation Filter for Video Coding. IEEE Transactions on Image Processing, 2019, 28, 4912-4925.   | 9.8  | 18        |
| 193 | Novel nanoscale control on soot formation by local CO2 micro-injection in ethylene inverse diffusion flames. Energy, 2019, 179, 697-708.  | 8.8  | 16        |
| 194 | Selective photoelectrochemical oxidation of glycerol to high value-added dihydroxyacetone. Nature Communications, 2019, 10, 1779.   | 12.8 | 185       |
| 195 | B-Spline-Based Sharp Feature Preserving Shape Reconstruction Approach for Electrical Impedance<br>Tomography. IEEE Transactions on Medical Imaging, 2019, 38, 2533-2544.  | 8.9  | 41        |
| 196 | Deficiency of mitophagy receptor FUNDC1 impairs mitochondrial quality and aggravates dietary-induced obesity and metabolic syndrome. Autophagy, 2019, 15, 1882-1898.  | 9.1  | 131       |
| 197 | Fabricating I doped TiO2 photoelectrode for the degradation of diclofenac: Performance and mechanism study. Chemical Engineering Journal, 2019, 369, 968-978.   | 12.7 | 37        |
| 198 | Traffic surveillance video coding with libraries of vehicles and background. Journal of Visual<br>Communication and Image Representation, 2019, 60, 426-440.  | 2.8  | 14        |

| #   | Article  | IF   | CITATIONS |
|-----|--|------|-----------|
| 199 | Enhanced Corrosion Resistance and Photocatalytic Properties of Bi2O3/Phosphate Composite Film<br>Prepared on AZ91D Magnesium Alloy by Phosphating. International Journal of Electrochemical Science,<br>2019, , 1434-1450.           | 1.3  | 4         |
| 200 | Effects of water addition on soot properties in ethylene inverse diffusion flames. Fuel, 2019, 247, 187-197.   | 6.4  | 47        |
| 201 | Expression analysis of the aquaporins during zebrafish embryonic development. Gene Expression Patterns, 2019, 32, 38-43.   | 0.8  | 8         |
| 202 | Breaking the symmetry: Gradient in NiFe layered double hydroxide nanoarrays for efficient oxygen evolution. Nano Energy, 2019, 60, 661-666.  | 16.0 | 52        |
| 203 | Chemical Approaches to Carbonâ€Based Metalâ€Free Catalysts. Advanced Materials, 2019, 31, e1804863.  | 21.0 | 90        |
| 204 | Noncontact direct temperature and concentration profiles measurement of soot and metal-oxide<br>nanoparticles in optically thin/thick nanofluid fuel flames. International Journal of Heat and Mass<br>Transfer, 2019, 134, 237-249. | 4.8  | 11        |
| 205 | A Statistical Shape-Constrained Reconstruction Framework for Electrical Impedance Tomography. IEEE<br>Transactions on Medical Imaging, 2019, 38, 2400-2410.  | 8.9  | 49        |
| 206 | Plonaphacarus species (Acari, Oribatida, Phthiracaridae) from China with<br>descriptions of two new species and a key to Chinese species. Systematic and Applied Acarology, 2019,<br>24, 251.  | 0.5  | 3         |
| 207 | Zebrafish Embryo Vessel Segmentation Using a Novel Dual ResUNet Model. Computational Intelligence and Neuroscience, 2019, 2019, 1-14.  | 1.7  | 10        |
| 208 | Accurate Parameter Estimation of a Hydro-Turbine Regulation System Using Adaptive Fuzzy Particle<br>Swarm Optimization. Energies, 2019, 12, 3903.  | 3.1  | 14        |
| 209 | Analysis of global three-dimensional aerosol structure with spectral radiance matching. Atmospheric<br>Measurement Techniques, 2019, 12, 6541-6556.  | 3.1  | 6         |
| 210 | Detrimental Effects and Prevention of Acidic Electrolytes on Oxygen Reduction Reaction Catalytic<br>Performance of Heteroatom-Doped Graphene Catalysts. Frontiers in Materials, 2019, 6, .   | 2.4  | 6         |
| 211 | The effects of Bi <sub>2</sub> O <sub>3</sub> on the selective catalytic reduction of NO by propylene over Co <sub>3</sub> O <sub>4</sub> nanoplates. RSC Advances, 2019, 9, 32232-32239.  | 3.6  | 10        |
| 212 | STING directly activates autophagy to tune the innate immune response. Cell Death and Differentiation, 2019, 26, 1735-1749.  | 11.2 | 247       |
| 213 | Experimental study on soot formation, evolution and characteristics of diffusion ethylene/air flames in Ĩ^-shaped mesoscale combustors. Fuel, 2019, 241, 138-154.  | 6.4  | 18        |
| 214 | NiFe Hydroxide Lattice Tensile Strain: Enhancement of Adsorption of Oxygenated Intermediates for<br>Efficient Water Oxidation Catalysis. Angewandte Chemie, 2019, 131, 746-750.  | 2.0  | 55        |
| 215 | Clustered Regularly Interspaced Short Palindromic Repeats (CRISPR)/Cas9â€mediated <i>kif15</i><br>mutations accelerate axonal outgrowth during neuronal development and regeneration in zebrafish.<br>Traffic, 2019, 20, 71-81.      | 2.7  | 15        |
| 216 | Genetic Dissection of Fe-Dependent Signaling in Root Developmental Responses to Phosphate<br>Deficiency. Plant Physiology, 2019, 179, 300-316.   | 4.8  | 72        |

| #   | Article  | IF   | CITATIONS |
|-----|--|------|-----------|
| 217 | One-for-All: Grouped Variation Network-Based Fractional Interpolation in Video Coding. IEEE<br>Transactions on Image Processing, 2019, 28, 2140-2151.  | 9.8  | 55        |
| 218 | Use of nanoparticles Cu/TiO(OH) <sub>2</sub> for CO <sub>2</sub> removal with<br>K <sub>2</sub> CO <sub>3</sub> /KHCO <sub>3</sub> based solution: enhanced thermal conductivity<br>and reaction kinetics enhancing the CO <sub>2</sub> sorption/desorption performance of<br>K <sub>2</sub> CO <sub>3</sub> /KHCO <sub>3</sub> ., 2019, 9, 10-18. |      | 4         |
| 219 | Dominant-Current Deep Learning Scheme for Electrical Impedance Tomography. IEEE Transactions on Biomedical Engineering, 2019, 66, 2546-2555.   | 4.2  | 109       |
| 220 | A ribosomal DNA-hosted microRNA regulates zebrafish embryonic angiogenesis. Angiogenesis, 2019, 22, 211-221.   | 7.2  | 11        |
| 221 | Treatment of efficiency for temperature and concentration profiles reconstruction of soot and metal-oxide nanoparticles in nanofluid fuel flames. International Journal of Heat and Mass Transfer, 2019, 133, 494-499.   | 4.8  | 4         |
| 222 | Mesoporous Carbon and Ceria Nanoparticles Composite Modified Electrode for the Simultaneous Determination of Hydroquinone and Catechol. Nanomaterials, 2019, 9, 54.  | 4.1  | 14        |
| 223 | Misalignment correction for free-form surface in non-null interferometric testing. Optics Communications, 2019, 437, 204-213.  | 2.1  | 6         |
| 224 | Influence of self-absorption on reconstruction accuracy for temperature and concentration profiles of soot and metal-oxide nanoparticles in asymmetric nanofluid fuel flames. Optik, 2019, 178, 740-751.   | 2.9  | 5         |
| 225 | Prescribed Performance Model-Free Adaptive Integral Sliding Mode Control for Discrete-Time<br>Nonlinear Systems. IEEE Transactions on Neural Networks and Learning Systems, 2019, 30, 2222-2230.   | 11.3 | 63        |
| 226 | Convolutional Neural Network-Based Block Up-Sampling for HEVC. IEEE Transactions on Circuits and Systems for Video Technology, 2019, 29, 3701-3715.  | 8.3  | 46        |
| 227 | Feature extraction of rotor fault based on EEMD and curve code. Measurement: Journal of the International Measurement Confederation, 2019, 135, 712-724.   | 5.0  | 35        |
| 228 | Learning a Convolutional Neural Network for Image Compact-Resolution. IEEE Transactions on Image Processing, 2019, 28, 1092-1107.  | 9.8  | 87        |
| 229 | Convolutional Neural Network-Based Fractional-Pixel Motion Compensation. IEEE Transactions on Circuits and Systems for Video Technology, 2019, 29, 840-853.  | 8.3  | 64        |
| 230 | Reference Clip for Inter Prediction in Video Coding. IEEE Transactions on Circuits and Systems for Video Technology, 2019, 29, 130-143.  | 8.3  | 6         |
| 231 | Data-Driven Adaptive Sliding Mode Control of Nonlinear Discrete-Time Systems With Prescribed<br>Performance. IEEE Transactions on Systems, Man, and Cybernetics: Systems, 2019, 49, 2598-2604.   | 9.3  | 59        |
| 232 | Design of a high-spectral-resolution lidar for atmospheric temperature measurement down to the near ground. Applied Optics, 2019, 58, 9651.  | 1.8  | 9         |
| 233 | Performance estimation of space-borne high-spectral-resolution lidar for cloud and aerosol optical properties at 532 nm. Optics Express, 2019, 27, A481.   | 3.4  | 19        |
| 234 | Phase function effects on the retrieval of oceanic high-spectral-resolution lidar. Optics Express, 2019, 27, A654.   | 3.4  | 14        |

| #   | Article  | IF  | CITATIONS |
|-----|--|-----|-----------|
| 235 | Retrieving the microphysical properties of opaque liquid water clouds from CALIOP measurements.<br>Optics Express, 2019, 27, 34126.  | 3.4 | 5         |
| 236 | Universal phase reconstruction approach of self-calibrating phase-shifting interferometry. Optics<br>Letters, 2019, 44, 3857.  | 3.3 | 9         |
| 237 | Multiple scattering effects on the return spectrum of oceanic high-spectral-resolution lidar. Optics Express, 2019, 27, 30204.   | 3.4 | 4         |
| 238 | A Parametric Level Set Method for Electrical Impedance Tomography. IEEE Transactions on Medical<br>Imaging, 2018, 37, 451-460.   | 8.9 | 70        |
| 239 | Image Denoising via Low Rank Regularization Exploiting Intra and Inter Patch Correlation. IEEE<br>Transactions on Circuits and Systems for Video Technology, 2018, 28, 3321-3332.  | 8.3 | 20        |
| 240 | Metastasis-associated miR-23a from nasopharyngeal carcinoma-derived exosomes mediates angiogenesis by repressing a novel target gene TSGA10. Oncogene, 2018, 37, 2873-2889.  | 5.9 | 154       |
| 241 | Hypoxia-Induced Matrix Metalloproteinase-13 Expression in Exosomes from Nasopharyngeal Carcinoma<br>Enhances Metastases. Cell Death and Disease, 2018, 9, 382.   | 6.3 | 92        |
| 242 | Three-dimensional BiOI/TiO2 heterostructures with photocatalytic activity under visible light<br>irradiation. Journal of Porous Materials, 2018, 25, 1805-1812.  | 2.6 | 18        |
| 243 | Effects of swirling combustion on soot characteristics in 2,5-dimethylfuran/n-heptane diffusion flames. Applied Thermal Engineering, 2018, 139, 11-24.   | 6.0 | 26        |
| 244 | Direct simultaneous reconstruction for temperature and concentration profiles of soot and<br>metal-oxide nanoparticles in nanofluid fuel flames by a CCD camera. International Journal of Heat and<br>Mass Transfer, 2018, 124, 564-575.   | 4.8 | 17        |
| 245 | Nanostructure and reactivity of carbon particles from co-pyrolysis of biodiesel surrogate methyl octanoate blended with <i>n</i> -butanol. Fullerenes Nanotubes and Carbon Nanostructures, 2018, 26, 278-290.  | 2.1 | 17        |
| 246 | SpyCatcher-N <sup>TEV</sup> : A Circularly Permuted, Disordered SpyCatcher Variant for Less Trace<br>Ligation. Bioconjugate Chemistry, 2018, 29, 1622-1629.  | 3.6 | 14        |
| 247 | Thermodynamic and economic analyses of a novel coal pyrolysis–gasification–combustion staged conversion utilization polygeneration system. Asia-Pacific Journal of Chemical Engineering, 2018, 13, e2171.  | 1.5 | 15        |
| 248 | Study of Sewage Sludge/Coal Co-Combustion by Thermogravimetric Analysis and Single Particle<br>Co-Combustion Method. Energy & Fuels, 2018, 32, 6300-6308.  | 5.1 | 24        |
| 249 | Effects of self-absorption on simultaneous estimation of temperature distribution and concentration fields of soot and metal-oxide nanoparticles in nanofluid fuel flames using a spectrometer. Journal of Quantitative Spectroscopy and Radiative Transfer, 2018, 212, 149-159. | 2.3 | 11        |
| 250 | Fast Image Super-Resolution via Local Adaptive Gradient Field Sharpening Transform. IEEE Transactions on Image Processing, 2018, 27, 1966-1980.  | 9.8 | 31        |
| 251 | Effects of Flame Configuration and Soot Aging on Soot Nanostructure and Reactivity in<br><i>n</i> Butanol-Doped Ethylene Diffusion Flames. Energy & Fuels, 2018, 32, 607-624.  | 5.1 | 38        |
| 252 | A Conductive Binder for High-Performance Sn Electrodes in Lithium-Ion Batteries. ACS Applied<br>Materials & Interfaces, 2018, 10, 1672-1677.   | 8.0 | 40        |

| #   | Article  | IF                | CITATIONS          |
|-----|--|-------------------|--------------------|
| 253 | Soot reduction by addition of dimethyl carbonate in normal and inverse ethylene diffusion flames:<br>Nanostructural evidence. Journal of Environmental Sciences, 2018, 72, 107-117.  | 6.1               | 25                 |
| 254 | Improvement in the mechanical properties, proton conductivity, and methanol resistance of highly branched sulfonated poly(arylene ether)/graphene oxide grafted with flexible alkylsulfonated side chains nanocomposite membranes. Journal of Power Sources, 2018, 378, 451-459. | 7.8               | 46                 |
| 255 | Energy conversion and ignition of fluffy graphene by flash light. Energy, 2018, 144, 669-678.  | 8.8               | 13                 |
| 256 | Functionalization of graphene materials by heteroatom-doping for energy conversion and storage.<br>Progress in Natural Science: Materials International, 2018, 28, 121-132.  | 4.4               | 148                |
| 257 | Enhanced visible light photoelectrocatalytic degradation of organic contaminants by F and Sn<br>co-doped TiO2 photoelectrode. Chemical Engineering Journal, 2018, 344, 332-341.  | 12.7              | 62                 |
| 258 | 100 MW Peak Power Picosecond Laser Based on Hybrid End-Pumped Nd:YVO4 and Side-Pumped Nd:YAG<br>Amplifiers. IEEE Journal of Selected Topics in Quantum Electronics, 2018, 24, 1-7.   | 2.9               | 12                 |
| 259 | On the treatment of self-absorption for temperature and concentration profiles reconstruction accuracy for soot and metal-oxide nanoparticles in nanofluid fuel flame using a CCD camera. Optik, 2018, 164, 114-125.   | 2.9               | 14                 |
| 260 | Effects of carbon nanotubes additions on flash ignition characteristics of Fe and Al nanoparticles.<br>Fullerenes Nanotubes and Carbon Nanostructures, 2018, 26, 168-174.  | 2.1               | 9                  |
| 261 | An Efficient Four-Parameter Affine Motion Model for Video Coding. IEEE Transactions on Circuits and Systems for Video Technology, 2018, 28, 1934-1948.   | 8.3               | 73                 |
| 262 | A Three-Dimensional Culture System with Matrigel Promotes Purified Spiral Ganglion Neuron Survival and Function In Vitro. Molecular Neurobiology, 2018, 55, 2070-2084.   | 4.0               | 46                 |
| 263 | Convolutional Neural Network-Based Block Up-Sampling for Intra Frame Coding. IEEE Transactions on<br>Circuits and Systems for Video Technology, 2018, 28, 2316-2330.   | 8.3               | 103                |
| 264 | Rotating a half-wave plate by 45°: An ideal calibration method for the gain ratio in polarization lidars.<br>Optics Communications, 2018, 407, 361-366.  | 2.1               | 5                  |
| 265 | Mechanism of core discing in the relaxation zone around an underground opening under high in situ stresses. Bulletin of Engineering Geology and the Environment, 2018, 77, 1179-1189.  | 3.5               | 11                 |
| 266 | Soot in flame-wall interactions: Views from nanostructure and reactivity. Fuel, 2018, 212, 117-131.  | 6.4               | 20                 |
| 267 | Inverse radiation analysis for simultaneous reconstruction of temperature and volume fraction<br>fields of soot and metal-oxide nanoparticles in a nanofluid fuel sooting flame. International Journal<br>of Heat and Mass Transfer, 2018, 118, 1080-1089.                       | 4.8               | 35                 |
| 268 | pH-sensitive zwitterionic coating of gold nanocages improves tumor targeting and photothermal treatment efficacy. Nano Research, 2018, 11, 3193-3204.  | 10.4              | 53                 |
| 269 | Contribution to the knowledge of the oribatid mite genus Mesoplophora (Acari: Oribatida:) Tj ETQq1 1 0.784314<br>1215-1221.  | ł rgBT /Ov<br>1.5 | erlock 10 Til<br>O |
| 270 | Effects of hydrogen addition on nanostructure and reactivity of carbon particles in flame–wall<br>interactions. Fullerenes Nanotubes and Carbon Nanostructures, 2018, 26, 756-764.   | 2.1               | 7                  |

| #   | Article  | IF   | CITATIONS |
|-----|--|------|-----------|
| 271 | An Intrinsically Disordered Peptide-Peptide Stapler for Highly Efficient Protein Ligation Both <i>in<br/>Vivo</i> and <i>in Vitro</i> . Journal of the American Chemical Society, 2018, 140, 17474-17483.  | 13.7 | 36        |
| 272 | Reply to Comments by Jia Yue on "Global Distribution and Variations of NO Infrared Radiative Flux and<br>Its Responses to Solar Activity and Geomagnetic Activity in the Thermosphere― Journal of Geophysical<br>Research: Space Physics, 2018, 123, 10,419. | 2.4  | 0         |
| 273 | Combustion characteristics and synergy behaviors of biomass and coal blending in oxy-fuel conditions: A single particle co-combustion method. Science China Technological Sciences, 2018, 61, 1723-1731.   | 4.0  | 14        |
| 274 | Two new species of the genus Indotritia (Acari, Oribatida, Oribotritiidae) from China with a key to<br>Chinese species. Systematic and Applied Acarology, 2018, 23, 1879.  | 0.5  | 1         |
| 275 | Phthiracarus species (Acari, Oribatida, Phthiracaridae) from Northeast China with descriptions of two new species and a key to Chinese species. Systematic and Applied Acarology, 2018, 23, 1817.  | 0.5  | 1         |
| 276 | New Zealand Austrophthiracarus (Acari, Oribatida, Steganacaridae): two new species from the North<br>Island. Zootaxa, 2018, 4500, 443.   | 0.5  | 3         |
| 277 | MIB1 mutations reduce Notch signaling activation and contribute to congenital heart disease. Clinical Science, 2018, 132, 2483-2491.   | 4.3  | 23        |
| 278 | Two new species of the genus Mesotritia (Acari: Oribatida: Oribotritiidae) from China. International<br>Journal of Acarology, 2018, 44, 395-399.   | 0.7  | 2         |
| 279 | Effects of an electrospun fluorinated poly(ether ether ketone) separator on the enhanced safety and electrochemical properties of lithium ion batteries. Electrochimica Acta, 2018, 290, 150-164.  | 5.2  | 48        |
| 280 | Nanoscale Characteristics and Reactivity of Nascent Soot from n-Heptane/2,5-Dimethylfuran Inverse<br>Diffusion Flames with/without Magnetic Fields. Energies, 2018, 11, 1698.  | 3.1  | 19        |
| 281 | Study on healing technique for weak interlayer and related mechanical properties based on microbially-induced calcium carbonate precipitation. PLoS ONE, 2018, 13, e0203834.   | 2.5  | 8         |
| 282 | Simultaneous reconstruction of temperature and concentration profiles of soot and metal-oxide<br>nanoparticles in asymmetric nanofluid fuel flames by inverse analysis. Journal of Quantitative<br>Spectroscopy and Radiative Transfer, 2018, 219, 174-185.  | 2.3  | 16        |
| 283 | Effects of dimethyl ether addition on soot formation, evolution and characteristics in flame-wall interactions. Energy, 2018, 164, 642-654.  | 8.8  | 22        |
| 284 | Checklist of oribatid mites (Acari, Oribatida) of the Russian Far East and Northeast of China. Zootaxa, 2018, 4472, 201.   | 0.5  | 14        |
| 285 | Failure Mechanism of Highly Stressed Rock Mass during Unloading Based on the Stress Arch Theory.<br>International Journal of Geomechanics, 2018, 18, 04018146.   | 2.7  | 9         |
| 286 | Semi-Supervised Community Detection Based on Distance Dynamics. IEEE Access, 2018, 6, 37261-37271.   | 4.2  | 23        |
| 287 | Novel design of photoelectrochemical device by dual BiVO4 photoelectrode with abundant oxygen vacancy. Science Bulletin, 2018, 63, 1027-1028.  | 9.0  | 4         |
| 288 | Branched comb-shaped poly(arylene ether sulfone)s containing flexible alkyl imidazolium side chains<br>as anion exchange membranes. Journal of Materials Chemistry A, 2018, 6, 10879-10890.  | 10.3 | 88        |

| #   | Article  | IF   | CITATIONS |
|-----|--|------|-----------|
| 289 | Mesoporous implantable Pt/SrTiO3:C,N nanocuboids delivering enhanced photocatalytic<br>H2-production activity via plasmon-induced interfacial electron transfer. Applied Catalysis B:<br>Environmental, 2018, 236, 338-347.                                  | 20.2 | 35        |
| 290 | Nanostructure evolution and reactivity of nascent soot from inverse diffusion flames in CO2, N2, and He atmospheres. Carbon, 2018, 139, 172-180.   | 10.3 | 66        |
| 291 | Reconstruction model for temperature and concentration profiles of soot and metal-oxide<br>nanoparticles in a nanofluid fuel flame by using a CCD camera. Chinese Physics B, 2018, 27, 054401.   | 1.4  | 13        |
| 292 | Spatial distribution patterns of soil mite communities and their relationships with edaphic factors in a 30-year tillage cornfield in northeast China. PLoS ONE, 2018, 13, e0199093.   | 2.5  | 6         |
| 293 | Effects of alkali and alkaline earth metal species on the combustion characteristics of single particles from pine sawdust and bituminous coal. Bioresource Technology, 2018, 268, 278-285.  | 9.6  | 47        |
| 294 | Catalogue of ptyctimous mites (Acari, Oribatida) of the world. Zootaxa, 2018, 4393, 1.   | 0.5  | 33        |
| 295 | Assessing the depolarization capabilities of nonspherical particles in a super-ellipsoidal shape space.<br>Optics Express, 2018, 26, 1726.   | 3.4  | 57        |
| 296 | ICF target DT-layer refractive index and thickness from iterative analysis. Optics Express, 2018, 26, 17781.   | 3.4  | 6         |
| 297 | N-desorption or NH3 generation of TiO2-loaded Al-based nitrogen carrier during chemical looping<br>ammonia generation technology. International Journal of Hydrogen Energy, 2018, 43, 16589-16597.   | 7.1  | 31        |
| 298 | Effects of branching structures on the properties of phosphoric acid-doped polybenzimidazole as a<br>membrane material for high-temperature proton exchange membrane fuel cells. International Journal<br>of Hydrogen Energy, 2018, 43, 16694-16703.         | 7.1  | 44        |
| 299 | Dimethyl Carbonate as a Promising Oxygenated Fuel for Combustion: A Review. Energies, 2018, 11, 1552.  | 3.1  | 70        |
| 300 | Four-layer metallodielectric emitter for spectrally selective near-field radiative transfer in nano-gap thermophotovoltaics. Journal of Quantitative Spectroscopy and Radiative Transfer, 2018, 217, 235-242.  | 2.3  | 13        |
| 301 | The Preparation, Characterization and Formation Mechanism of a Calcium Phosphate Conversion<br>Coating on Magnesium Alloy AZ91D. Materials, 2018, 11, 908.   | 2.9  | 22        |
| 302 | The expression of natriuretic peptide receptors in developing zebrafish embryos. Gene Expression Patterns, 2018, 29, 65-71.  | 0.8  | 12        |
| 303 | Seedâ€5urface Grafting Precipitation Polymerization for Preparing Microsized Optically Active Helical<br>Polymer Core/Shell Particles and Their Application in Enantioselective Crystallization.<br>Macromolecular Rapid Communications, 2018, 39, e1800072. | 3.9  | 7         |
| 304 | Effects of auxiliary atmospheric state parameters on the aerosol optical properties retrieval errors of high-spectral-resolution lidar. Applied Optics, 2018, 57, 2627.  | 1.8  | 10        |
| 305 | Dry Reforming of Shale Gas and Carbon Dioxide with Niâ€Ceâ€Al <sub>2</sub> O <sub>3</sub> Catalyst:<br>Syngas Production Enhanced over Niâ€CeO <sub>x</sub> Formation. ChemCatChem, 2018, 10, 4689-4698.   | 3.7  | 31        |
| 306 | Synthesis of Amorphous Carbon Film in Ethanol Inverse Diffusion Flames. Nanomaterials, 2018, 8, 656.   | 4.1  | 4         |

| #   | Article   | IF   | CITATIONS |
|-----|---|------|-----------|
| 307 | Planar Metasurfaces Enable Highâ€Efficiency Colored Perovskite Solar Cells. Advanced Science, 2018, 5,<br>1800836.  | 11.2 | 33        |
| 308 | Healing Technique for Rock Cracks Based on Microbiologically Induced Calcium Carbonate<br>Mineralization. Journal of Materials in Civil Engineering, 2018, 30, .  | 2.9  | 7         |
| 309 | A Parametric Level set Method for Imaging Multiphase Conductivity Using Electrical Impedance<br>Tomography. IEEE Transactions on Computational Imaging, 2018, 4, 552-561.   | 4.4  | 41        |
| 310 | First-principles and experimental studies of [ZrO(OH)] <sup>+</sup> or ZrO(OH) <sub>2</sub> for<br>enhancing CO <sub>2</sub> desorption kinetics – imperative for significant reduction of<br>CO <sub>2</sub> capture energy consumption. Journal of Materials Chemistry A, 2018, 6, 17671-17681. | 10.3 | 13        |
| 311 | Relationship between the effective attenuation coefficient of spaceborne lidar signal and the IOPs of seawater. Optics Express, 2018, 26, 30278.  | 3.4  | 19        |
| 312 | A pressure-tuned field-widened Michelson interferometer system as the spectroscopic filter of high-spectral-resolution lidar. , 2018, , .   |      | 0         |
| 313 | Structure of Macrobenthic Assemblages and Its Relationship with Environmental Variables in the East<br>China Sea of Xiangshan. Pakistan Journal of Zoology, 2018, 51, .   | 0.2  | 0         |
| 314 | Reflectance Reference for Intra-Frame Coding of Surveillance Video. Lecture Notes in Computer Science, 2018, , 481-491.   | 1.3  | 1         |
| 315 | A Convolutional Neural Network Approach for Post-Processing in HEVC Intra Coding. Lecture Notes in Computer Science, 2017, , 28-39.   | 1.3  | 211       |
| 316 | Effects of multi-orifice configurations of the quench plate on mixing characteristics of the quench zone in an RQL-TVC model. Experimental Thermal and Fluid Science, 2017, 83, 57-68.  | 2.7  | 27        |
| 317 | Motives Matter: Motives for Playing Pokémon Go and Implications for Well-Being. Cyberpsychology,<br>Behavior, and Social Networking, 2017, 20, 52-57.   | 3.9  | 100       |
| 318 | Geochronology and geochemistry of the Early Jurassic Yeba Formation volcanic rocks in southern<br>Tibet: Initiation of back-arc rifting and crustal accretion in the southern Lhasa Terrane. Lithos, 2017,<br>278-281, 477-490.   | 1.4  | 89        |
| 319 | Sub-nanometer planar solar absorber. Nano Energy, 2017, 34, 172-180.  | 16.0 | 23        |
| 320 | CYP6B6 is involved in esfenvalerate detoxification in the polyphagous lepidopteran pest, Helicoverpa armigera. Pesticide Biochemistry and Physiology, 2017, 138, 51-56.   | 3.6  | 36        |
| 321 | Novel conductive binder for high-performance silicon anodes in lithium ion batteries. Nano Energy, 2017, 36, 206-212.   | 16.0 | 178       |
| 322 | Pseudo Sequence Based 2-D Hierarchical Coding Structure for Light-Field Image Compression. , 2017, , .  |      | 23        |
| 323 | Accelerated simulation of the degradation process of poly(arylene ether ketone)s containing<br>alkylsulfonated side chains used as a proton exchange mmembrane. RSC Advances, 2017, 7, 8994-9001.   | 3.6  | 9         |
| 324 | Effects of butanol isomers additions on soot nanostructure and reactivity in normal and inverse ethylene diffusion flames. Fuel, 2017, 205, 109-129.  | 6.4  | 77        |

| #   | Article   | IF   | CITATIONS |
|-----|---|------|-----------|
| 325 | Combustion characteristics of nanofluid fuels in a half-opening slot tube. Science China<br>Technological Sciences, 2017, 60, 1075-1087.  | 4.0  | 12        |
| 326 | An episomal vector-based CRISPR/Cas9 system for highly efficient gene knockout in human pluripotent stem cells. Scientific Reports, 2017, 7, 2320.  | 3.3  | 91        |
| 327 | Catalytic pyrolysis and gasification of waste textile under carbon dioxide atmosphere with composite<br>Zn-Fe catalyst. Fuel Processing Technology, 2017, 166, 115-123.   | 7.2  | 23        |
| 328 | Nobleâ€Metalâ€Free Janusâ€like Structures by Cation Exchange for Zâ€Scheme Photocatalytic Water Splitting<br>under Broadband Light Irradiation. Angewandte Chemie - International Edition, 2017, 56, 4206-4210.   | 13.8 | 166       |
| 329 | Nobleâ€Metalâ€Free Janusâ€like Structures by Cation Exchange for Zâ€&cheme Photocatalytic Water Splitting<br>under Broadband Light Irradiation. Angewandte Chemie, 2017, 129, 4270-4274.  | 2.0  | 62        |
| 330 | Recognizable or Not: Towards Image Semantic Quality Assessment for Compression. Sensing and Imaging, 2017, 18, 1.   | 1.5  | 18        |
| 331 | Fine-Grained Image Recognition from Click-Through Logs Using Deep Siamese Network. Lecture Notes in Computer Science, 2017, , 127-138.  | 1.3  | 4         |
| 332 | Understanding the mechanism of improvement in practical specific capacity using halogen substituted anthraquinones as cathode materials in lithium batteries. Electrochimica Acta, 2017, 224, 622-627.  | 5.2  | 9         |
| 333 | Leucogranites in Lhozag, southern Tibet: Implications for the tectonic evolution of the eastern<br>Himalaya. Lithos, 2017, 294-295, 246-262.  | 1.4  | 38        |
| 334 | Autophagy protects auditory hair cells against neomycin-induced damage. Autophagy, 2017, 13, 1884-1904.   | 9.1  | 195       |
| 335 | Improving triplet-wise training of convolutional neural network for vehicle re-identification. , 2017, ,  |      | 69        |
| 336 | Vegfa signaling regulates diverse artery/vein formation in vertebrate vasculatures. Journal of<br>Genetics and Genomics, 2017, 44, 483-492.   | 3.9  | 22        |
| 337 | Fe <sub>2</sub> O <sub>3</sub> , a cost effective and environmentally friendly catalyst for the generation of NH <sub>3</sub> – a future fuel – using a new Al <sub>2</sub> O <sub>3</sub> -looping based technology. Chemical Communications, 2017, 53, 10664-10667. | 4.1  | 31        |
| 338 | Facile Processing of Free-Standing Polyaniline/SWCNT Film as an Integrated Electrode for Flexible Supercapacitor Application. ACS Applied Materials & amp; Interfaces, 2017, 9, 33791-33801.  | 8.0  | 139       |
| 339 | A meta-analysis of the relationship of academic performance and Social Network Site use among adolescents and young adults. Computers in Human Behavior, 2017, 77, 148-157.   | 8.5  | 89        |
| 340 | Photoelectrocatalytic degradation of methylene blue using F doped TiO2 photoelectrode under visible light irradiation. Chemosphere, 2017, 185, 574-581.   | 8.2  | 82        |
| 341 | Density functional theory and reactive dynamics study of catalytic performance of TiO2 on CO2 desorption process with KHCO3/TiO2/Al2O3 sorbent. Molecular Catalysis, 2017, 439, 143-154.  | 2.0  | 14        |
| 342 | The effects of specific surface area and ash on char gasification mechanisms in the mixture of H2O, CO2, H2 and CO. Fuel, 2017, 209, 109-116.   | 6.4  | 27        |

| #   | Article   | IF   | CITATIONS       |
|-----|---|------|-----------------|
| 343 | A TBX5 3′UTR variant increases the risk of congenital heart disease in the Han Chinese population. Cell Discovery, 2017, 3, 17026.  | 6.7  | 23              |
| 344 | The Big Five personality traits, Big Two metatraits and social media: A meta-analysis. Journal of<br>Research in Personality, 2017, 70, 229-240.  | 1.7  | 144             |
| 345 | Energy conversion and ignition of iron nanoparticles by flash. Science China Technological Sciences, 2017, 60, 1878-1884.   | 4.0  | 11              |
| 346 | Silicon nanostructures for solar-driven catalytic applications. Nano Today, 2017, 17, 96-116.   | 11.9 | 63              |
| 347 | The pyrolysis and gasification performances of waste textile under carbon dioxide atmosphere.<br>Journal of Thermal Analysis and Calorimetry, 2017, 128, 581-591.   | 3.6  | 25              |
| 348 | Pseudo-Sequence-Based 2-D Hierarchical Coding Structure for Light-Field Image Compression. IEEE<br>Journal on Selected Topics in Signal Processing, 2017, 11, 1107-1119.  | 10.8 | 63              |
| 349 | Two new species of the genusEuphthiracarus(Acari: Oribatida: Euphthiracaridae) from Hainan Island,<br>China. International Journal of Acarology, 2017, 43, 450-455.   | 0.7  | 1               |
| 350 | Coupled chemical effects of carbon dioxide and hydrogen additions on premixed lean dimethyl ether flames. Science China Technological Sciences, 2017, 60, 102-115.<br>&Itspan style= font-size: 10px; >New species of the family Steganacaridae (Acari, Oribatida,) 1] ETQq1 10.7 | 4.0  | 8<br>Tiovarloch |
| 351 | style="font-size: 10px;">Austrophthiracarus <span style="font-size: 10px;"> and<br/></span> <em style="font-size: 10px;">Hoplophthiracarus<span style="font-size: 10px;"></span></em>   | 0.5  | 3               |
| 352 | Kinetic analysis of ethanol and dimethyl ether flames with hydrogen addition. International Journal of Hydrogen Energy, 2017, 42, 3813-3823.  | 7.1  | 22              |
| 353 | Expression of SoxC Transcription Factors during Zebrafish Retinal and Optic Nerve Regeneration.<br>Neuroscience Bulletin, 2017, 33, 53-61.  | 2.9  | 15              |
| 354 | Highly Crystalline Mesoporous Silicon Spheres for Efficient Visible Photocatalytic Hydrogen<br>Evolution. ChemNanoMat, 2017, 3, 22-26.  | 2.8  | 27              |
| 355 | Effects of hydrogen additions on premixed rich flames of four butanol isomers. International Journal of Hydrogen Energy, 2017, 42, 3833-3841.   | 7.1  | 23              |
| 356 | On the effects of hydrogen addition in premixed formaldehyde flames. International Journal of<br>Hydrogen Energy, 2017, 42, 3824-3832.  | 7.1  | 14              |
| 357 | Practical retrace error correction in non-null aspheric testing: A comparison. Optics<br>Communications, 2017, 383, 378-385.  | 2.1  | 17              |
| 358 | 3D-hybrid material design with electron/lithium-ion dual-conductivity for high-performance Li-sulfur<br>batteries. Journal of Power Sources, 2017, 340, 160-166.  | 7.8  | 28              |
| 359 | Generation of a mef2aa:EGFP transgenic zebrafish line that expresses EGFP in muscle cells. Fish<br>Physiology and Biochemistry, 2017, 43, 287-294.  | 2.3  | 9               |
| 360 | Block-Composed Background Reference for High Efficiency Video Coding. IEEE Transactions on<br>Circuits and Systems for Video Technology, 2017, 27, 2639-2651.   | 8.3  | 35              |

| #   | Article  | IF  | CITATIONS |
|-----|--|-----|-----------|
| 361 | A convolutional neural network approach for half-pel interpolation in video coding. , 2017, , .  |     | 45        |
| 362 | On-line fall detection via a boosted cascade of hybrid features. , 2017, , .   |     | 1         |
| 363 | The geochronologic and geochemical constraints on the Early Cretaceous subduction magmatism in the central Lhasa subterrane, Tibet. Geological Journal, 2017, 52, 463-475.               | 1.3 | 12        |
| 364 | Fatty Acid Binding Protein 11a Is Required for Brain Vessel Integrity in Zebrafish. Frontiers in Physiology, 2017, 8, 214.   | 2.8 | 5         |
| 365 | Polarization properties of receiving telescopes in atmospheric remote sensing polarization lidars.<br>Applied Optics, 2017, 56, 6837.  | 1.8 | 12        |
| 366 | Design of iodine absorption cell for high-spectral-resolution lidar. Optics Express, 2017, 25, 15913.  | 3.4 | 27        |
| 367 | Generalized high-spectral-resolution lidar technique with a multimode laser for aerosol remote sensing. Optics Express, 2017, 25, 979.   | 3.4 | 10        |
| 368 | Retrieving the seawater volume scattering function at the 180° scattering angle with a high-spectral-resolution lidar. Optics Express, 2017, 25, 11813.                                  | 3.4 | 15        |
| 369 | Use of Debye's series to determine the optimal edge-effect terms for computing the extinction efficiencies of spheroids. Optics Express, 2017, 25, 20298.                                | 3.4 | 13        |
| 370 | Nanostructure and Oxidation Reactivity of Nascent Soot Particles in Ethylene/Pentanol Flames.<br>Energies, 2017, 10, 122.  | 3.1 | 32        |
| 371 | On the Response of Nascent Soot Nanostructure and Oxidative Reactivity to Photoflash Exposure.<br>Energies, 2017, 10, 961.   | 3.1 | 14        |
| 372 | Combustion Characteristics of Single Particles from Bituminous Coal and Pine Sawdust in O2/N2, O2/CO2, and O2/H2O Atmospheres. Energies, 2017, 10, 1695.                                 | 3.1 | 35        |
| 373 | Insm1a Is Required for Zebrafish Posterior Lateral Line Development. Frontiers in Molecular<br>Neuroscience, 2017, 10, 241.  | 2.9 | 24        |
| 374 | Insm1a Regulates Motor Neuron Development in Zebrafish. Frontiers in Molecular Neuroscience, 2017,<br>10, 274.   | 2.9 | 42        |
| 375 | Fault diagnosis of rotor using EMD thresholding-based de-noising combined with probabilistic neural network. Journal of Vibroengineering, 2017, 19, 5920-5931.                           | 1.0 | 16        |
| 376 | Effects of a nonideal half-wave plate on the gain ratio calibration measurements in polarization<br>lidars. Applied Optics, 2017, 56, 8100.  | 1.8 | 1         |
| 377 | Three Dimensional Simulation of Electrical Impedance Tomography for Imaging Vocal Folds Within the<br>Human Neck. Journal of Medical Imaging and Health Informatics, 2017, 7, 1509-1516. | 0.3 | 0         |
| 378 | New and little known ptyctimous mites (Acari: Oribatida) with a key to known species of Oribotritia<br>from the Australasian Region. Biologia (Poland), 2016, 71, 917-923.               | 1.5 | 3         |

| #   | Article   | IF   | CITATIONS |
|-----|---|------|-----------|
| 379 | Antiviral Drug Ganciclovir Is a Potent Inhibitor of the Proliferation of Müller Glia–Derived<br>Progenitors During Zebrafish Retinal Regeneration. , 2016, 57, 1991.  |      | 9         |
| 380 | Hypoxic mitophagy regulates mitochondrial quality and platelet activation and determines severity of<br>I/R heart injury. ELife, 2016, 5, .   | 6.0  | 158       |
| 381 | Design of the interferometric spectral discrimination filters for a three-wavelength high-spectral-resolution lidar. Optics Express, 2016, 24, 27622.   | 3.4  | 5         |
| 382 | Social networking online and personality of self-worth: A meta-analysis. Journal of Research in Personality, 2016, 64, 79-89.   | 1.7  | 128       |
| 383 | Integration of Multiple Plasmonic and Co-Catalyst Nanostructures on TiO <sub>2</sub> Nanosheets<br>for Visible-Near-Infrared Photocatalytic Hydrogen Evolution. Small, 2016, 12, 1640-1648.   | 10.0 | 136       |
| 384 | Preparation of porous MoO <sub>2</sub> @C nano-octahedrons from a polyoxometalate-based<br>metal–organic framework for highly reversible lithium storage. Journal of Materials Chemistry A,<br>2016, 4, 12434-12441.  | 10.3 | 83        |
| 385 | A Meta-Analysis of Social Networking Online and Social Capital. Review of General Psychology, 2016, 20, 369-391.  | 3.2  | 129       |
| 386 | Combretastatin A-4 efficiently inhibits angiogenesis and induces neuronal apoptosis in zebrafish.<br>Scientific Reports, 2016, 6, 30189.  | 3.3  | 18        |
| 387 | Media Niche of Electronic Communication Channels in Friendship: A Meta-Analysis. Journal of<br>Computer-Mediated Communication, 2016, 21, 451-466.  | 3.3  | 58        |
| 388 | Hierarchical quadtree-based flexible block ordering in HEVC intra coding. , 2016, , .   |      | 7         |
| 389 | Pd-Ag alloy hollow nanostructures with interatomic charge polarization for enhanced electrocatalytic formic acid oxidation. Nano Research, 2016, 9, 1590-1599.  | 10.4 | 102       |
| 390 | The small-scale structure of a soil mite metacommunity. European Journal of Soil Biology, 2016, 74, 69-75.  | 3.2  | 15        |
| 391 | Field-widened Michelson interferometer for spectral discrimination in high-spectral-resolution lidar:<br>practical development. Optics Express, 2016, 24, 7232.   | 3.4  | 13        |
| 392 | Combustion characteristics of primary reference fuels with hydrogen addition. International Journal of Hydrogen Energy, 2016, 41, 11471-11480.  | 7.1  | 23        |
| 393 | 95-ps all-solid-state laser with a low-power microchip laser seed and a two-stage single-pass bounce<br>geometry amplifier. Journal of the Optical Society of America B: Optical Physics, 2016, 33, 884.  | 2.1  | 5         |
| 394 | Phthiracarusspecies (Acari: Oribatida: Phthiracaridae) from New Zealand, with description of a new<br>species, redescription ofPhthiracarus pellucidusand a key to 19 described species from the Australian<br>Region. Journal of Natural History, 2016, 50, 1463-1472. | 0.5  | 5         |
| 395 | Pseudo-sequence-based light field image compression. , 2016, , .  |      | 130       |
| 396 | Defects evaluation system for spherical optical surfaces based on microscopic scattering dark-field<br>imaging method. Applied Optics, 2016, 55, 6162.  | 2.1  | 38        |

| #   | Article  | IF   | CITATIONS |
|-----|--|------|-----------|
| 397 | Beam quality management by periodic reproduction of wavefront aberrations in end-pumped Nd:YVO_4<br>laser amplifiers. Optics Express, 2016, 24, 8988.  | 3.4  | 8         |
| 398 | Frequency locking of a field-widened Michelson interferometer based on optimal multi-harmonics heterodyning. Optics Letters, 2016, 41, 3916.   | 3.3  | 7         |
| 399 | Mesoplophoroidea (Acari, Oribatida) of China. Zootaxa, 2016, 4084, 519-39.   | 0.5  | 8         |
| 400 | Combining directional intra prediction and intra block copy with block partition for HEVC. , 2016, , .   |      | 6         |
| 401 | <inline-formula> <tex-math notation="LaTeX">\$lambda\$</tex-math><br/></inline-formula> -Domain Rate Control Algorithm for HEVC Scalable Extension. IEEE<br>Transactions on Multimedia, 2016, 18, 2023-2039. | 7.2  | 30        |
| 402 | Detection of trace levels of Pd2+ in pure water using a fluorescent probe assisted by surfactants.<br>Sensors and Actuators B: Chemical, 2016, 237, 899-904.   | 7.8  | 21        |
| 403 | Two new species of <i>Austrophthiracarus</i> (Acari: Oribatida: Phthiracaridae) from Capleston<br>Biological Reserve in New Zealand. International Journal of Acarology, 2016, 42, 416-419.                  | 0.7  | 4         |
| 404 | Multi-Scale Triplet CNN for Person Re-Identification. , 2016, , .  |      | 124       |
| 405 | NgAgo-based fabp11a gene knockdown causes eye developmental defects in zebrafish. Cell Research, 2016, 26, 1349-1352.  | 12.0 | 53        |
| 406 | Experimental study of inhibitor containing sulfur for mild steel in hydrochloric acid. Anti-Corrosion<br>Methods and Materials, 2016, 63, 275-280.   | 1.5  | 0         |
| 407 | The THO/TREX Complex Active in miRNA Biogenesis Negatively Regulates Root-Associated Acid<br>Phosphatase Activity Induced by Phosphate Starvation. Plant Physiology, 2016, 171, 2841-2853.                   | 4.8  | 16        |
| 408 | Minimizing cross-axis sensitivity in grating-based optomechanical accelerometers. Optics Express, 2016, 24, 9094.  | 3.4  | 40        |
| 409 | Synthesis and properties of highly branched polybenzimidazoles as proton exchange membranes for high-temperature fuel cells. Journal of Materials Chemistry C, 2016, 4, 4814-4821.                           | 5.5  | 58        |
| 410 | Enhanced full-spectrum water splitting by confining plasmonic Au nanoparticles in N-doped TiO2 bowl nanoarrays. Nano Energy, 2016, 24, 87-93.  | 16.0 | 118       |
| 411 | Preparation and properties of highly branched sulfonated poly(arylene ether)/polyacrylonitrile<br>composite materials as proton exchange membranes. Journal of Materials Science, 2016, 51, 7119-7129.       | 3.7  | 18        |
| 412 | The structural development of primary cultured hippocampal neurons on a graphene substrate.<br>Colloids and Surfaces B: Biointerfaces, 2016, 146, 442-451.   | 5.0  | 40        |
| 413 | Flexible Nearâ€Infrared Photovoltaic Devices Based on Plasmonic Hotâ€Electron Injection into Silicon<br>Nanowire Arrays. Angewandte Chemie, 2016, 128, 4653-4657.  | 2.0  | 7         |
| 414 | Flexible Nearâ€Infrared Photovoltaic Devices Based on Plasmonic Hotâ€Electron Injection into Silicon<br>Nanowire Arrays. Angewandte Chemie - International Edition, 2016, 55, 4577-4581.                     | 13.8 | 64        |

| #   | Article   | IF  | CITATIONS |
|-----|---|-----|-----------|
| 415 | Synthesis and properties of highly branched sulfonated poly(arylene ether)s with flexible<br>alkylsulfonated side chains as proton exchange membranes. Journal of Materials Chemistry C, 2016, 4,<br>1326-1335.   | 5.5 | 35        |
| 416 | Review of the genus <i>Austrophthiracarus</i> (Acari, Oribatida, Phthiracaridae) with a description of<br>a new species from Australia, a key to known species of the Australian Region and a world checklist.<br>International Journal of Acarology, 2016, 42, 41-55.  | 0.7 | 9         |
| 417 | Cooperative Nanoparticle System for Photothermal Tumor Treatment without Skin Damage. ACS<br>Applied Materials & Interfaces, 2016, 8, 2847-2856.  | 8.0 | 24        |
| 418 | Nonlinear Difference Imaging Approach to Three-Dimensional Electrical Impedance Tomography in the<br>Presence of Geometric Modeling Errors. IEEE Transactions on Biomedical Engineering, 2016, 63,<br>1956-1965.  | 4.2 | 56        |
| 419 | MicroRNA-10a/10b represses a novel target gene mib1 to regulate angiogenesis. Cardiovascular Research, 2016, 110, 140-150.  | 3.8 | 69        |
| 420 | Arabidopsis PHL2 and PHR1 Act Redundantly as the Key Components of the Central Regulatory System Controlling Transcriptional Responses to Phosphate Starvation. Plant Physiology, 2016, 170, 499-514.   | 4.8 | 155       |
| 421 | Social Diffusion Analysis With Common-Interest Model for Image Annotation. IEEE Transactions on<br>Multimedia, 2016, 18, 687-701.   | 7.2 | 20        |
| 422 | The somite-secreted factor Maeg promotes zebrafish embryonic angiogenesis. Oncotarget, 2016, 7,<br>77749-77763.   | 1.8 | 10        |
| 423 | Simultaneous reconstruction of temperature field and radiative properties by inverse radiation analysis using stochastic particle swarm optimization. Thermal Science, 2016, 20, 493-504.   | 1.1 | 14        |
| 424 | Practical phase unwrapping of interferometric fringes based on unscented Kalman filter technique.<br>Optics Express, 2015, 23, 32337.   | 3.4 | 58        |
| 425 | <p align="left" class="Body"><strong>Review of the genus <em>Acrotritia<br/></em>(Acari, Oribatida, Euphthiracaridae) with a world checklist, a key to known species of the<br/>Neotropical Region, and a description of a new species from Colombia</strong></p> .<br>Systematic and Applied Acarology, 2015, 20, 887. | 0.5 | 3         |
| 426 | Image semantic quality assessment for compression of car-plate images. , 2015, , .  |     | 2         |
| 427 | Coal Char Gasification on a Circulating Fluidized Bed for Hydrogen Generation: Experiments and Simulation. Energy Technology, 2015, 3, 1059-1067.   | 3.8 | 15        |
| 428 | Efficient background picture coding for videos obtained from static cameras. , 2015, , .  |     | 2         |
| 429 | <strong>Review of <em>Oribotritia</em> (Acari, Oribatida, Oribotritiidae) with a<br/>world checklist and description of a new species from China</strong> . Zootaxa, 2015, 4007, 217.   | 0.5 | 8         |
| 430 | <p><strong><em>Acrotritia</em> species (Acari: Oribatida: Euphthiracaridae)<br/>from China with description of a new species</strong></p> . Zootaxa, 2015, 3937, 127.   | 0.5 | 6         |
| 431 | Effective Semisupervised Community Detection Using Negative Information. Mathematical Problems in Engineering, 2015, 2015, 1-8.   | 1.1 | 2         |
| 432 | General measurement of optical system aberrations with a continuously variable lateral shear ratio<br>by a randomly encoded hybrid grating. Applied Optics, 2015, 54, 8913.   | 2.1 | 19        |

| #   | Article   | IF   | CITATIONS |
|-----|---|------|-----------|
| 433 | Highly sensitive lateral deformable optical MEMS displacement sensor: anomalous diffraction studied by rigorous coupled-wave analysis. Applied Optics, 2015, 54, 8935.  | 2.1  | 2         |
| 434 | Inter-picture prediction based on 3D point cloud model. , 2015, , .   |      | 6         |
| 435 | Detailed influences of ethanol as fuel additive on combustion chemistry of premixed fuel-rich ethylene flames. Science China Technological Sciences, 2015, 58, 1696-1704.                                     | 4.0  | 12        |
| 436 | Hoplophthiracarus species (Acari: Oribatida: Phthiracaridae) from China with descriptions of two<br>new species. Biologia (Poland), 2015, 70, 1490-1494.  | 1.5  | 3         |
| 437 | The Nature of Photocatalytic "Water Splitting―on Silicon Nanowires. Angewandte Chemie -<br>International Edition, 2015, 54, 2980-2985.  | 13.8 | 97        |
| 438 | Detailed influences of chemical effects of hydrogen as fuel additive on methane flame. International<br>Journal of Hydrogen Energy, 2015, 40, 3777-3788.  | 7.1  | 44        |
| 439 | Large-area synthesis of monolayer WSe <sub>2</sub> on a SiO <sub>2</sub> /Si substrate and its device applications. Nanoscale, 2015, 7, 4193-4198.  | 5.6  | 128       |
| 440 | The Nature of Photocatalytic "Water Splitting―on Silicon Nanowires. Angewandte Chemie, 2015, 127,<br>3023-3028.   | 2.0  | 7         |
| 441 | A nonlinear approach to difference imaging in EIT; assessment of the robustness in the presence of modelling errors. Inverse Problems, 2015, 31, 035012.  | 2.0  | 51        |
| 442 | Laminar flame propagation and ignition properties of premixed iso-octane/air with hydrogen addition.<br>Fuel, 2015, 158, 443-450.   | 6.4  | 49        |
| 443 | Chemical Effects of Carbon Dioxide Addition on Dimethyl Ether and Ethanol Flames: A Comparative<br>Study. Energy & Fuels, 2015, 29, 3385-3393.  | 5.1  | 21        |
| 444 | Multi-phase flow monitoring with electrical impedance tomography using level set based method.<br>Nuclear Engineering and Design, 2015, 289, 108-116.   | 1.7  | 25        |
| 445 | Birth Cohort and Age Changes in the Selfâ€Esteem of Chinese Adolescents: A Crossâ€Temporal<br>Metaâ€Analysis, 1996–2009. Journal of Research on Adolescence, 2015, 25, 366-376.                               | 3.7  | 40        |
| 446 | Egfl6 is involved in zebrafish notochord development. Fish Physiology and Biochemistry, 2015, 41, 961-969.  | 2.3  | 8         |
| 447 | Pd–Ag alloy nanocages: integration of Ag plasmonic properties with Pd active sites for light-driven catalytic hydrogenation. Journal of Materials Chemistry A, 2015, 3, 9390-9394.                            | 10.3 | 29        |
| 448 | Three new species of the genus <i>Notophthiracarus</i> (Acari: Oribatida: Phthiracaridae), with an<br>updated key to its known species in New Zealand. International Journal of Acarology, 2015, 41, 232-240. | 0.7  | 6         |
| 449 | Determination of aspheric vertex radius of curvature in non-null interferometry. Applied Optics, 2015, 54, 2838.  | 1.8  | 16        |
| 450 | Pattern recognition model for aerosol classification with atmospheric backscatter lidars: principles<br>and simulations. Journal of Applied Remote Sensing, 2015, 9, 096006.                                  | 1.3  | 12        |

| #   | Article  | IF          | CITATIONS      |
|-----|--|-------------|----------------|
| 451 | Field-widened Michelson interferometer for spectral discrimination in high-spectral-resolution lidar:<br>theoretical framework. Optics Express, 2015, 23, 12117.   | 3.4         | 27             |
| 452 | Aspheric subaperture stitching based on system modeling. Optics Express, 2015, 23, 19176.  | 3.4         | 28             |
| 453 | Three-Dimensional Point-Cloud Plus Patches: Towards Model-Based Image Coding in the Cloud. , 2015, , .   |             | 5              |
| 454 | Quadriwave lateral shearing interferometer based on a randomly encoded hybrid grating. Optics Letters, 2015, 40, 2245.   | 3.3         | 40             |
| 455 | Two new species of the family Phthiracaridae (Acari, Oribatida) from New Zealand, including keys to<br>all species ofPlonaphacarusandArphthicarusof the Australian region. International Journal of<br>Acarology, 2015, 41, 584-589. | 0.7         | 5              |
| 456 | Identifying mantle carbonatite metasomatism through Os–Sr–Mg isotopes in Tibetan ultrapotassic<br>rocks. Earth and Planetary Science Letters, 2015, 430, 458-469.  | 4.4         | 82             |
| 457 | Block the function of nonmuscle myosin II by blebbistatin induces zebrafish embryo cardia bifida. In<br>Vitro Cellular and Developmental Biology - Animal, 2015, 51, 211-217.  | 1.5         | 3              |
| 458 | <strong>New Zealand </strong> <strong><em>Austrophthiracarus<br/></em>(Acari: Oribatida: Phthiracaridae): three new species from North Island and offshore<br/>islands</strong> . Systematic and Applied Acarology, 2015, 20, 263.   | 0.5         | 9              |
| 459 | Estimation of conductivity changes in a region of interest with electrical impedance tomography.<br>Inverse Problems and Imaging, 2015, 9, 211-229.  | 1.1         | 43             |
| 460 | Three new species of the genus <em>Notophthiracarus</em> from New Zealand (Acari:) Tj ETQq0 0 0  | rgBT/Ove    | rlogck 10 Tf 5 |
| 461 | Three new species of the genus Austrophthiracarus from New Zealand (Acari: Oribatida:) Tj ETQq1 1 0.784314 rg  | gBT /Overlo | ock 10 Tf 50   |
| 462 | Two new species of phthiracarid mites (Acari, Oribatida, Phthiracaridae) from Queensland, Australia.<br>International Journal of Acarology, 2014, 40, 247-253.   | 0.7         | 2              |
| 463 | First record of the genus <i>Arphthicarus</i> NiedbaÅ,a (Acari: Oribatida: Phthiracaridae) from China,<br>with descriptions of two new species. Journal of Natural History, 2014, 48, 2199-2206.                                     | 0.5         | 4              |
| 464 | Kinesinâ€12 influences axonal growth during zebrafish neural development. Cytoskeleton, 2014, 71,<br>555-563.  | 2.0         | 39             |
| 465 | Outage Analysis of Dual-Hop Transmission with Buffer Aided Amplify-and-Forward Relay. , 2014, , .  |             | 13             |
| 466 | Zircon xenocrysts in Tibetan ultrapotassic magmas: Imaging the deep crust through time. Geology, 2014, 42, 43-46.  | 4.4         | 85             |
| 467 | SIFT-preserving compression of mobile-captured license plate images for recognition. , 2014, , .   |             | 3              |
| 468 | Effects of spectral discrimination in high-spectral-resolution lidar on the retrieval errors for atmospheric aerosol optical properties. Applied Optics, 2014, 53, 4386.   | 1.8         | 29             |

| #   | Article   | IF  | CITATIONS |
|-----|---|-----|-----------|
| 469 | Non-null annular subaperture stitching interferometry for steep aspheric measurement. Applied Optics, 2014, 53, 5755.   | 1.8 | 36        |
| 470 | Reverse optimization reconstruction of aspheric figure error in a non-null interferometer. Applied Optics, 2014, 53, 5538.  | 1.8 | 36        |
| 471 | Common-path and compact wavefront diagnosis system based on cross grating lateral shearing interferometer. Applied Optics, 2014, 53, 7144.  | 1.8 | 24        |
| 472 | Two new peculiar ptyctimous mites (Acari: Oribatida: Phthiracaridae) from the Australian region, with<br>a key to 54 described species of <i>Notophthiracarus</i> â€Ramsay in Australia. Austral Entomology, 2014,<br>53, 159-166.          | 1.4 | 8         |
| 473 | Optically active helical polyacetylene/Fe <sub>3</sub> O <sub>4</sub> composite microspheres:<br>prepared by precipitation polymerization and used for enantioselective crystallization. RSC Advances,<br>2014, 4, 63611-63619.             | 3.6 | 22        |
| 474 | <i>Microtritia</i> species from China (Acari: Oribatida: Euphthiracaridae), with description of a new species and a world key to species of the genus. International Journal of Acarology, 2014, 40, 402-409.                               | 0.7 | 6         |
| 475 | Two new species of oribatid mites of the family Phthiracaridae (Acari, Oribatida) from Venezuela.<br>International Journal of Acarology, 2014, 40, 443-448.   | 0.7 | 4         |
| 476 | Category-based dynamic recommendations adaptive to user interest drifts. , 2014, , .  |     | 5         |
| 477 | Descriptions of Two New Species of <i>Austrophthiracarus</i> Balogh et Mahunka, a Newly Recorded<br>Genus of Ptyctimous Mites from China (Acari: Oribatida: Phthiracaridae). Annales Zoologici, 2014, 64,<br>267-272.                       | 0.8 | 8         |
| 478 | Postcollisional potassic and ultrapotassic rocks in southern Tibet: Mantle and crustal origins in response to India–Asia collision and convergence. Geochimica Et Cosmochimica Acta, 2014, 143, 207-231.                                    | 3.9 | 187       |
| 479 | Helix-sense-selective polymerization of achiral substituted acetylene in chiral micelles for preparing optically active polymer nanoparticles: Effects of chiral emulsifiers. Polymer, 2014, 55, 840-847.                                   | 3.8 | 17        |
| 480 | Characterization of NADPH–cytochrome P450 reductase gene from the cotton bollworm, Helicoverpa<br>armigera. Gene, 2014, 545, 262-270.   | 2.2 | 18        |
| 481 | A Facile Method for Preparing Porous, Optically Active, Magnetic<br>Fe <sub>3</sub> O <sub>4</sub> @poly( <i>N</i> â€acryloylâ€keucine) Inverse Core/Shell Composite<br>Microspheres. Macromolecular Rapid Communications, 2014, 35, 91-96. | 3.9 | 9         |
| 482 | Redescription ofAustrotritia lebronneci(Oribotritiidae) and descriptions of two new species of<br>Euphthiracaridae (Acari, Oribatida) from Australian Region. International Journal of Acarology, 2014,<br>40, 43-51.                       | 0.7 | 11        |
| 483 | Visualization of user interests in online music services. , 2014, , .   |     | 0         |
| 484 | Expression analysis of integrin β1 isoforms during zebrafish embryonic development. Gene Expression<br>Patterns, 2014, 16, 86-92.   | 0.8 | 10        |
| 485 | Image annotation via social diffusion analysis with common interests. , 2014, , .   |     | 1         |
| 486 | Relative roles of spatial factors, environmental filtering and biotic interactions in fine-scale structuring of a soil mite community. Soil Biology and Biochemistry, 2014, 79, 68-77.  | 8.8 | 54        |

| #   | Article   | IF         | CITATIONS    |
|-----|---|------------|--------------|
| 487 | lldr1b is essential for semicircular canal development, migration of the posterior lateral line primordium and hearing ability in zebrafish: implications for a role in the recessive hearing impairment DFNB42. Human Molecular Genetics, 2014, 23, 6201-6211. | 2.9        | 16           |
| 488 | Self-disclosure on social networking sites, positive feedback, and social capital among Chinese college students. Computers in Human Behavior, 2014, 38, 213-219.   | 8.5        | 116          |
| 489 | Kinetic analysis of the chemical effects of hydrogen addition on dimethyl ether flames. International<br>Journal of Hydrogen Energy, 2014, 39, 13014-13019.   | 7.1        | 43           |
| 490 | Automated discrimination between digs and dust particles on optical surfaces with dark-field scattering microscopy. Applied Optics, 2014, 53, 5131.   | 1.8        | 39           |
| 491 | Co-occurrence patterns of above-ground and below-ground mite communities in farmland of Sanjiang<br>Plain, Northeast China. Chinese Geographical Science, 2014, 24, 339-347.  | 3.0        | 3            |
| 492 | Northward subduction of Bangong–Nujiang Tethys: Insight from Late Jurassic intrusive rocks from<br>Bangong Tso in western Tibet. Lithos, 2014, 205, 284-297.  | 1.4        | 140          |
| 493 | Combustion chemistry and flame structure of furan group biofuels using molecular-beam mass<br>spectrometry and gas chromatography – Part III: 2,5-Dimethylfuran. Combustion and Flame, 2014, 161,<br>780-797.   | 5.2        | 127          |
| 494 | Distortion correction in surface defects evaluating system of large fine optics. Optics<br>Communications, 2014, 312, 110-116.  | 2.1        | 21           |
| 495 | Origin of the ca. 90 Ma magnesia-rich volcanic rocks in SE Nyima, central Tibet: Products of<br>lithospheric delamination beneath the Lhasa-Qiangtang collision zone. Lithos, 2014, 198-199, 24-37.   | 1.4        | 106          |
| 496 | Combustion chemistry and flame structure of furan group biofuels using molecular-beam mass<br>spectrometry and gas chromatography – Part II: 2-Methylfuran. Combustion and Flame, 2014, 161,<br>766-779.  | 5.2        | 110          |
| 497 | Combustion chemistry and flame structure of furan group biofuels using molecular-beam mass spectrometry and gas chromatography – Part I: Furan. Combustion and Flame, 2014, 161, 748-765.   | 5.2        | 117          |
| 498 | <em>Atropacarus (Hoplophorella)</em> species (Acari: Oribatida: Phthiracaridae) from China, with descriptions of two new species. Systematic and Applied Acarology, 2014, 19, 166.  | 0.5        | 6            |
| 499 | <em>Phthiracarus</em> species from China with descriptions of three new speciesÂ(Acari:) Tj ETQq1 1   | 0.784314   | 4 ggBT /Over |
| 500 | Vision-based tomographic reconstruction of emissivity distribution in asymmetric thermal plasma.<br>Europhysics Letters, 2013, 103, 35002.  | 2.0        | 0            |
| 501 | Optically Active Particles of Chiral Polymers. Macromolecular Rapid Communications, 2013, 34, 1426-1445.  | 3.9        | 48           |
| 502 | Atropacarus(Atropacarus)niedbalaisp. nov., an extreme case of neotrichy in oribatid mites (Acari:) Tj ETQq0 0 0 rg  | BT /Overlo | ock 10 Tf 50 |
| 503 | Optically active, magnetic gels consisting of helical substituted polyacetylene and Fe3O4<br>nanoparticles: preparation and chiral recognition ability. Journal of Materials Chemistry C, 2013, 1,<br>8066.   | 5.5        | 30           |

<sup>504</sup> miR-30a Regulates Endothelial Tip Cell Formation and Arteriolar Branching. Hypertension, 2013, 62, 2.7 62

| #   | Article   | IF  | CITATIONS |
|-----|---|-----|-----------|
| 505 | Two new species of the genus <i>Notophthiracarus</i> (Acari: Oribatida: Phthiracaridae) from China.<br>International Journal of Acarology, 2013, 39, 418-422.   | 0.7 | 3         |
| 506 | New Species of Oribatid Mites of the Families Parakalummidae and Galumnidae (Acari: Oribatida) from<br>Xiao Hinggan Mountains, Northeastern China. Annales Zoologici, 2013, 63, 171-176.  | 0.8 | 2         |
| 507 | Nonmuscle myosin II-B (myh10) expression analysis during zebrafish embryonic development. Gene<br>Expression Patterns, 2013, 13, 265-270.   | 0.8 | 44        |
| 508 | Flame structure and kinetic studies of carbon dioxide-diluted dimethyl ether flames at reduced and elevated pressures. Combustion and Flame, 2013, 160, 2654-2668.  | 5.2 | 95        |
| 509 | Oribatid mites from Wanda Mountains in China, with description of a new species of the genus <i>Pilogalumna</i> . International Journal of Acarology, 2013, 39, 414-417.  | 0.7 | 3         |
| 510 | Off-axis cyclic radial shearing interferometer for measurement of centrally blocked transient wavefront. Optics Letters, 2013, 38, 2493.  | 3.3 | 17        |
| 511 | Dark-field microscopic image stitching method for surface defects evaluation of large fine optics.<br>Optics Express, 2013, 21, 5974.   | 3.4 | 68        |
| 512 | Retrieval and analysis of a polarized high-spectral-resolution lidar for profiling aerosol optical properties. Optics Express, 2013, 21, 13084.   | 3.4 | 52        |
| 513 | Interferometric filters for spectral discrimination in high-spectral-resolution lidar: performance<br>comparisons between Fabry–Perot interferometer and field-widened Michelson interferometer.<br>Applied Optics, 2013, 52, 7838. | 1.8 | 21        |
| 514 | Practical and accurate method for aspheric misalignment aberrations calibration in non-null interferometric testing. Applied Optics, 2013, 52, 8501.  | 1.8 | 31        |
| 515 | Research on the Stability of Surrounding Rock in Shallow Tunnel under Unsymmetrical Pressure<br>Based on RDM. Applied Mechanics and Materials, 2013, 353-356, 1709-1712.  | 0.2 | 0         |
| 516 | Research on Optimization of Excavating Seguence for Dawangou Tunnel. Applied Mechanics and Materials, 2013, 353-356, 3703-3706.   | 0.2 | 0         |
| 517 | Three new species of the genus <i>Suctobelbella</i> (Acari: Oribatida: Suctobelbidae) from<br>Sanjiang Plain, Northeast China. Zootaxa, 2013, 3637, 131-8.  | 0.5 | 4         |
| 518 | New Zealand species of <i>Oribotritia</i> (Acari: Oribatida: Oribotritiidae): descriptions of<br>two new species and a key to eight species. Systematic and Applied Acarology, 2013, 18, 153.                                       | 0.5 | 9         |
| 519 | Hotspots of new species discovery: new mite species described during 2007 to 2012. Zootaxa, 2013, 3663, 1.  | 0.5 | 23        |
| 520 | Two new species of <i>Austrophthiracarus</i> (Acari: Oribatida: Phthiracaridae) from New<br>Zealand. Zootaxa, 2013, 3682, 385-91.   | 0.5 | 17        |
| 521 | The genus <i>Notophthiracarus</i> of New Zealand (Acari: Oribatida: Phthiracaridae): three new species and a key to 24 described species. Zootaxa, 2013, 3682, 392-400.   | 0.5 | 13        |
|     |   |     |           |

<strong&gt;&lt;strong&gt;&lt;/strong&gt;&lt;/strong&gt;&lt;p align="justify"&gt;Two new species of the genus <em&gt;Phrathicarus&lt;/em&gt; from New Zealand (Acari: Oribatida:) Tj ETQq0 0 0 rgBT /Overlock 100.650 57 #d (Phthirac

| #   | Article   | IF             | CITATIONS |
|-----|---|----------------|-----------|
| 523 | 纳米晶ä¼2"在电å,¬åŒ−甲é,æ°§åŒ−å应ä,çš,,形貌效应. Scientia Sinica Chimica, 2013, 43, 744-   | 75 <b>8.</b> 4 | 3         |
| 524 | Differential Gene Expression Profiling and Biological Process Analysis in Proximal Nerve Segments after Sciatic Nerve Transection. PLoS ONE, 2013, 8, e57000.   | 2.5            | 67        |
| 525 | НарруGо. , 2012, , .  |                | 5         |
| 526 | System analysis of a tilted field-widened Michelson interferometer for high spectral resolution lidar.<br>Optics Express, 2012, 20, 1406.   | 3.4            | 39        |
| 527 | Towards Annotating Media Contents through Social Diffusion Analysis. , 2012, , .  |                | 17        |
| 528 | Soot Optical Properties in the Terahertz Spectra Domain. Journal of Heat Transfer, 2012, 134, .   | 2.1            | 1         |
| 529 | Poly(N-propargylamide)s bearing cholesteryl moieties: Preparation and optical activity. Reactive and Functional Polymers, 2012, 72, 832-838.  | 4.1            | 11        |
| 530 | Six new species of the genus Euphthiracarus (Acari: Oribatida: Euphthiracaridae) from China. Zootaxa,<br>2012, 3481, 47.  | 0.5            | 10        |
| 531 | Magnetic Fe <sub>3</sub> O <sub>4</sub> â€PSâ€Polyacetylene Composite Microspheres Showing Chirality<br>Derived From Helical Substituted Polyacetylene. Macromolecular Rapid Communications, 2012, 33,<br>672-677.    | 3.9            | 32        |
| 532 | Solar energy conversion with tunable plasmonic nanostructures for thermoelectric devices.<br>Nanoscale, 2012, 4, 4416.  | 5.6            | 53        |
| 533 | Experimental reconstructions of flame temperature distributions in laboratory-scale and large-scale pulverized-coal fired furnaces by inverse radiation analysis. Fuel, 2012, 93, 397-403.                            | 6.4            | 55        |
| 534 | On the treatment of non-optimal regularization parameter influence on temperature distribution reconstruction accuracy in participating medium. International Journal of Heat and Mass Transfer, 2012, 55, 1553-1560. | 4.8            | 18        |
| 535 | Inpainting with image patches for compression. Journal of Visual Communication and Image Representation, 2012, 23, 100-113.   | 2.8            | 41        |
| 536 | Descriptions of Two New Species of the Family Oribotritiidae (Acari: Oribatida: Euphthiracaroidea).<br>Annales Zoologici, 2011, 61, 811-816.  | 0.8            | 5         |
| 537 | The role of blood flow and microRNAs in blood vessel development. International Journal of Developmental Biology, 2011, 55, 419-429.  | 0.6            | 21        |
| 538 | Synthesis and characterization of magnetic Fe3O4-silica-poly(γ-benzyl-l-glutamate) composite microspheres. Reactive and Functional Polymers, 2011, 71, 1040-1044.   | 4.1            | 30        |
| 539 | On the treatment of scattering for three-dimensional temperature distribution reconstruction accuracy in participating medium. International Journal of Heat and Mass Transfer, 2011, 54, 1684-1687.                  | 4.8            | 19        |
| 540 | Preparation of optically active poly(N-propargylamide) gels and their application in chiral recognition. Macromolecular Research, 2011, 19, 729-733.  | 2.4            | 11        |

| #   | Article   | IF                | CITATIONS        |
|-----|---|-------------------|------------------|
| 541 | Flt1 acts as a negative regulator of tip cell formation and branching morphogenesis in the zebrafish embryo. Development (Cambridge), 2011, 138, 2111-2120.   | 2.5               | 142              |
| 542 | Neuron navigator 3a regulates liver organogenesis during zebrafish embryogenesis. Development<br>(Cambridge), 2011, 138, 1935-1945.   | 2.5               | 24               |
| 543 | Review of Plonaphacarus (Acari: Oribatida: Steganacaridae), with descriptions of eight new species<br>from China. Zootaxa, 2011, 2739, .  | 0.5               | 16               |
| 544 | Species of Euphthiracarus (Acari: Oribatida: Euphthiracaridae) from China. Zootaxa, 2011, 2752, .   | 0.5               | 6                |
| 545 | Critical role of connexin43 in zebrafish late primitive and definitive hematopoiesis. Fish Physiology and Biochemistry, 2010, 36, 945-951.  | 2.3               | 5                |
| 546 | Birth cohort changes of Chinese adolescents' anxiety: A cross-temporal meta-analysis, 1992–2005.<br>Personality and Individual Differences, 2010, 48, 208-212.  | 2.9               | 54               |
| 547 | Simultaneous measurements of two-dimensional temperature and particle concentration distribution from the image of the pulverized-coal flame. Fuel, 2010, 89, 202-211.  | 6.4               | 44               |
| 548 | <strong>Oribatid mites of China: a review of progress, with a checklist</strong> .<br>Zoosymposia, 2010, 4, 186-224.  | 0.3               | 35               |
| 549 | A review of Mesotritia (Acari: Oribatida: Oribotritiidae) in China, with descriptions of two new species and a checklist of known taxa. Zootaxa, 2010, 2479, 39.  | 0.5               | 5                |
| 550 | Review of Apoplophora (Acari: Oribatida: Mesoplophoridae), with the description of a new species from China. Zootaxa, 2009, 2051, 49-61.  | 0.5               | 6                |
| 551 | A new species ofSabahtritia(Acari: Oribatida: Synichotritiidae) from China. Oriental Insects, 2009, 43,<br>361-374.   | 0.3               | 3                |
| 552 | Reconstruction of soot temperature and volume fraction profiles of an asymmetric flame using stereoscopic tomography. Combustion and Flame, 2009, 156, 565-573.   | 5.2               | 91               |
| 553 | yap is required for the development of brain, eyes, and neural crest in zebrafish. Biochemical and<br>Biophysical Research Communications, 2009, 384, 114-119.  | 2.1               | 46               |
| 554 | Practical methods for retrace error correction in nonnull aspheric testing. Optics Express, 2009, 17, 7025.   | 3.4               | 64               |
| 555 | Improving Inverse Wavelet Transform by Compressive Sensing Decoding with Deconvolution. , 2009, , .   |                   | 2                |
| 556 | Review of Austrotritia (Acari: Oribatida: Oribotritiidae), with descriptions of two new species from<br>China. Zootaxa, 2009, 2144, 54-64.  | 0.5               | 3                |
| 557 | Taxonomic Study of the Genus <l>Maerkelotritia</l> Hammer, 1967 (Acari: Oribatida:) Tj ETQq1 1 0.7  | 784314 rgB<br>0.8 | T /Overlock<br>2 |
| 558 | Efficient inverse radiation analysis of temperature distribution in participating medium based on<br>backward Monte Carlo method. Journal of Quantitative Spectroscopy and Radiative Transfer, 2008,<br>109, 2171-2181. | 2.3               | 44               |

| #   | Article  | IF  | CITATIONS |
|-----|--|-----|-----------|
| 559 | Improvement of Load-Following Capacity Based on the Flame Radiation Intensity Signal in a Power<br>Plant. Energy & Fuels, 2008, 22, 1731-1738.   | 5.1 | 13        |
| 560 | Noncontact temperature measurement by means of CCD cameras in a participating medium. Optics Letters, 2008, 33, 422.   | 3.3 | 39        |
| 561 | Intra Prediction via Edge-Based Inpainting. Proceedings of the Data Compression Conference, 2008, , .  | 0.0 | 9         |
| 562 | Edge-Oriented Uniform Intra Prediction. IEEE Transactions on Image Processing, 2008, 17, 1827-1836.  | 9.8 | 27        |
| 563 | The effect of acetic acid and acetate on CO <sub>2</sub> corrosion of carbon steel. Anti-Corrosion Methods and Materials, 2008, 55, 130-134.   | 1.5 | 21        |
| 564 | Manipulating image patches for compression. , 2008, , .  |     | 1         |
| 565 | Measurement of Three-Dimensional Temperature Distribution in an Absorbing, Emitting, and Anisotropically Scattering Medium. AIP Conference Proceedings, 2007, , .  | 0.4 | 1         |
| 566 | Real time diagnosis of transient pulse laser with high repetition by radial shearing interferometer.<br>Applied Optics, 2007, 46, 8305.  | 2.1 | 40        |
| 567 | Image Compression With Edge-Based Inpainting. IEEE Transactions on Circuits and Systems for Video Technology, 2007, 17, 1273-1287.   | 8.3 | 152       |
| 568 | Measurement of transient near-infrared laser pulse wavefront with high precision by radial shearing interferometer. Optics Communications, 2007, 275, 173-178.   | 2.1 | 18        |
| 569 | Microscopic scattering imaging measurement and digital evaluation system of defects for fine optical surface. Optics Communications, 2007, 278, 240-246.   | 2.1 | 58        |
| 570 | Simulation study on radiative imaging of combustion flame in furnace. Journal of Zhejiang University:<br>Science A, 2007, 8, 1853-1857.  | 2.4 | 2         |
| 571 | A novel fuzzy classification entropy approach to image thresholding. Pattern Recognition Letters, 2006, 27, 1968-1975.   | 4.2 | 46        |
| 572 | Numerical Simulation of Advanced Small Pipe in Tunnels during Excavation by Steps. Applied Mechanics and Materials, 0, 353-356, 3699-3702.   | 0.2 | 2         |
| 573 | Study on Fluid-Structure Interaction Based on Hard Rock Deterioration Theory. Applied Mechanics and Materials, 0, 353-356, 1551-1554.  | 0.2 | 0         |
| 574 | Study on the Ground Settlement Regularity Caused by Deep Caving Method. Applied Mechanics and Materials, 0, 670-671, 907-911.  | 0.2 | 1         |
| 575 | The Structure and Composition of Corrosion Product Film and its Relation to Corrosion Rate for<br>Carbon Steels in CO2 Saturated Solutions at Different Temperatures. Journal of the Brazilian<br>Chemical Society, 0, , . | 0.6 | 8         |
| 576 | Study of Cool Flames of Octane Isomers in the Counterflow Burner. Combustion Science and Technology, 0, , 1-15.  | 2.3 | 1         |